A-dependence of Φ meson production at HERA-B

A Dissertation

Presented to the Faculty of the Department of Physics

University of Houston

In Partial Fulfillment

of the Requirements for the Degree

Doctor of Philosophy

By

Mikayel Ispiryan

May 2004

A-dependence of Φ meson production at HERA-B

Mikayel Ispiryan

APPROVED:

Dr. Kwong Lau, Chairman

Dr. David Bao

Dr. Ed Hungerford

Dr. Roy Weinstein

Dean, College of Natural Sciences and Mathematics

ACKNOWLEDGEMENTS

This work is a result of joint efforts of many physicists, engineers, programmers involved in HERA-B, to whom I am very grateful.

I am especially thankful to my scientific advisor Dr. Kwong Lau for his guidance and support of my work as well as education. He shared his experience and knowledge, leading the work to its completion.

I would also like to thank senior colleagues from DESY Prof. Roy Schwitters, Prof. Robert Avakian, Prof. Jerry Rosen and Dr. Andreas Schwarz, from whom I have learned valuable professional skills.

My special thanks to colleagues at DESY Kendall Reeves, Reinhard Eckmann, Suren Karabekyan, Sergey Essenov, Birgit Lewendel, Alexander Lanyov, and Halasya-Siva Subramania from the University of Houston, who kindly assisted me with advice, examples, suggestions, and who shared their methods and results.

A-dependence of Φ meson production at HERA-B

An Abstract of a Dissertation

Presented to

the Faculty of the Department of Physics

University of Houston

In Partial Fulfillment

of the Requirements for the Degree

Doctor of Philosophy

By

Mikayel Ispiryan

May 2004

ABSTRACT

In the HERA-B experiment at DESY, Germany, 920 GeV protons collide with nuclei of the targets. In the collisions many hadrons are produced and detected by the spectrometer, allowing the study of various issues of hadron-hadron and hadron-nucleus interactions. In this thesis the production dependence of the Φ meson on the atomic weight A of the nuclei has been studied for several materials, with the goal of obtaining experimental information on proton-nucleus (p-A) interactions. For this, runs and events have been selected according to special criteria. The Φ meson's signature - its decay into two charged kaons - has been used to detect the fact of the production of a Φ meson in the collision. The RICH detector, the tracking system, and selection algorithms have been used for identification of kaons. The main result, obtaining of which does not depend on the knowledge of integrated luminosity and does not depend heavily on the Monte Carlo simulation of the spectrometer, is the exponent $\Delta\alpha$ of the power law of the Φ meson production cross-section in an inelastic interaction: $\sigma \propto A^{\Delta\alpha}$, which was measured to be 0.14 .. 0.19 for tungsten, titanium and rhenium, with $\Delta\alpha = 0.141 \pm 0.012(stat) \pm 0.022(sys)$ being the most exact number obtained from the analysis of ~10^8 events on carbon and tungsten targets. As a by-product, the mass of the Φ meson is obtained to be 1.01957 GeV, which did not show dependence on the type of the target nucleus within statistical error of approximately ± 80 keV. The results show a clear experimental indication of A-dependence for Φ meson production in proton-nucleon inelastic interactions.

Table of Contents

Chapter 1. Proton-nucleus collisions

1.1. The goals of this work

The HERA-B experiment at DESY (Deutsches Elektronen-Synchrotron), Germany, provided an opportunity to study the dependence of Φ meson production on the atomic weight A of the nuclei (A-dependence) in proton-nucleus (p-A) collisions at 920 GeV due to the following unique features of the experiment:

1) usage of several different target materials;
2) large acceptance; and
3) relatively large sample of reconstructed Φ mesons (around 4000).

The goal of this work was to exploit these opportunities to obtain the A-dependence of Φ meson production per inelastic interaction. There are several benefits in experimentally obtaining the nuclear dependence of particle production. First, it is one more method to study nuclear matter. Second, the experimentally obtained dependence can be used for comparing these data to theoretical investigations (mainly in the form of rejecting some of the multitude of models suggested). Third, it is useful for the planning of future experiments. There are, of course, other benefits as well.

Obtaining the A-dependence of the cross-section per inelastic interaction, as opposed to obtaining the A-dependence of the cross-section, allows us to perform a relative measurement which eliminated most of systematic uncertainties associated with

cross-section measurements. The survey of the available experimental papers indicates that there are no data on A-dependence of Φ meson production at the HERA-B energy 920 GeV ($\sqrt{s} = 41.6$ GeV). In 4.4, we present the exponent of A-dependence of Φ meson production at 120 GeV, obtained in another experiment.

1.2. Features of the Standard Model

The Standard Model (SM) of elementary particles, widely accepted today, describes very well most properties and interactions of elementary particles [1]. According to the SM, all elementary particles are divided into two groups: leptons and quarks. Leptons are subject only to electromagnetic and weak interactions, whereas quarks also participate in strong interactions. Interactions in the SM are mediated through exchange of spin 1 particles (gluons, photon, heavy bosons), called gauge bosons. Table 1 summarizes the particles of the SM.

Table 1. Elementary particles in the Standard Model.

Leptons and quarks (fermions)				***Gauge bosons***	
Generation	***1***	***2***	***3***	***Interaction***	***Carrier particle(s)***
Leptons	e ν_e	μ ν_μ	τ ν_τ	Strong	8 gluons (g)
Quarks	u d	c s	t b	Electromagnetic	photon (γ)
				Weak	$W^{\pm}, Z^0$

A peculiar property of the quarks is that they are confined - they are bound inside the hadrons (hadrons are the strongly interacting particles), and do not exist outside of hadrons. Any attempt to liberate a single quark from inside a hadron, for example by means of a high energy collision with another hadron, yields only quark-antiquark or quark-quark-quark bound states.

Quark doublets consist of quark-antiquark pairs $q\overline{q}$, called mesons. Examples are: the Φ meson consisting of an $s\overline{s}$ pair; the J/Ψ meson consisting of a $c\overline{c}$ pair; the D^0 meson consisting of a $c\overline{u}$ pair. (In particle physics, "consist of" is used with great caution; it often means that the composite particle possesses the algebraic sum of corresponding quantum numbers of the more elementary particles). Baryons - the other type of hadrons - consist of quark triplets. Examples are the proton (uud) and the neutron (udd).

At any given time, the quark constituents within hadrons interact with one other. This necessarily means that gluons are also present inside the hadrons, since they are the carriers of strong interactions among quarks. Gluons bind the quarks together. Thus the simplest model of hadrons contains quarks and gluons, together referred to as partons. Leptons do not contain partons; in fact, in the SM they do not have a structure. This makes them an effective tool to study the internal structure of the hadrons.

The partons must be held together, to create a hadron. There are several models of how this could be possible. One simple and often used model is the MIT bag model [2], which suggests that non-interacting partons are inside a bag (a potential bag). The bag exerts enough pressure over partons so that they cannot escape. Another model is the

elastic potential model: if the attractive force between partons increases linearly with distance (elastic force), then the partons cannot escape since the force will become infinitely large at large distances.

These models are, of course, simplified. Quantum Chromodynamics (QCD), which is the theory for strong interactions, develops the picture further. In a high-energy hadron-hadron collision, quarks are predominantly produced in the collision of two partons - one from the target and one from the projectile. In this interaction, the relative movements of partons within each of the colliding hadrons can be neglected. At HERA-B energies of 920 GeV the internal movements and interactions of the partons play an insignificant role [3]. The most important strong interaction processes occurring during the collision are the gluon-gluon fusion: $g+g \rightarrow q+\overline{q}$ and quark-antiquark annihilation: $q_a+\overline{q_a} \rightarrow q_b+\overline{q_b}$. To calculate the total cross-section of a process in QCD, one must sum the interactions over all parton types and take the integral over the kinematic region. Very often the wavefunctions or other quantities required for this calculation are unknown, and theories, besides putting forward models of an interaction, must hypothesize about the exact form of the unknown functions. Usually there are several theories describing a nontrivial hadronic interaction.

Fig. 1 shows schematically the geometrical interpretation of a peripheral proton-neutron (p-n) collision. In this particular collision, two gluon-gluon interactions are possible: g3-g4 or g3-g5. Other partons are unlikely to interact, since they are far from one another. In other words, their wavefunctions do not overlap significantly. Models like this are often used to understand interactions. We will use them to qualitatively understand the propagation of an $s\overline{s}$ pair through nuclear media.

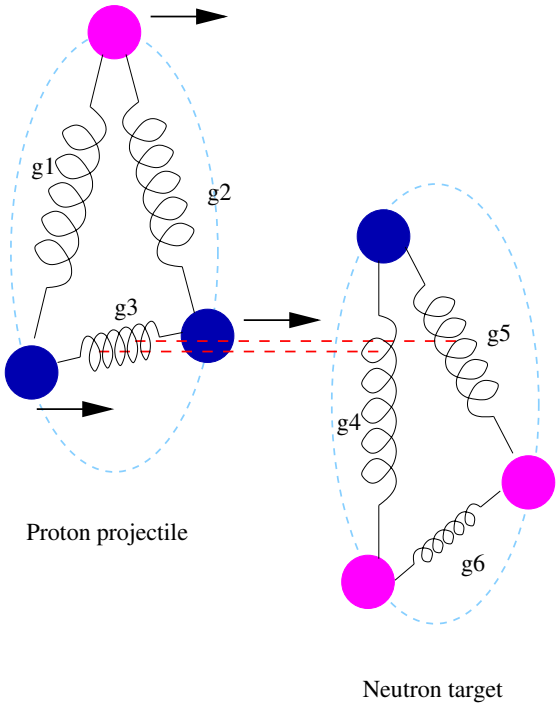

Fig. 1. A schematic picture of proton-neutron collision. Gluon g3 might interact with one of the gluons g4 or g5. Other partons are spectators.

1.3. Particle interactions in proton-nucleus collisions

The collision of two hadrons thus looks like collision of two bags of partons. Depending on the geometry of collision, some partons interact and some do not. Those that interact (the valence quarks), interact on one-on-one basis. The others that do not interact (the spectator quarks) may participate later in hadronization process to form hadrons of the final state.

The picture of p-A collision has a lot in common with the picture of hadron-hadron

collision. The model analogous to the bag model is called the Glauber model. Glauber models (there are several of them) [4] stipulate that hadron-nucleus collisions take place in the same way that partons interact in the bag model; namely, the whole interaction is the sum of constituents' interactions. For instance, in case of a proton projectile and a nuclear target, as shown in Fig. 2, the interacting constituents will be the projectile and the nucleons #2, 3, 4, 5, 6, 7. The other nucleons are spectators.

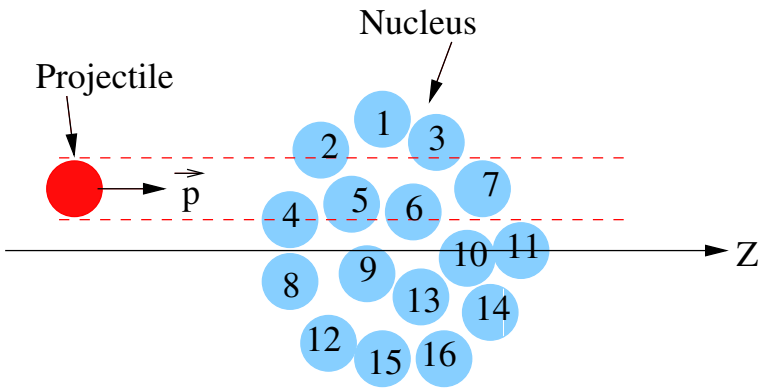

Fig. 2. Proton-nucleus collision according to the Glauber model.

It appears that often the major part of the total p-A interaction takes place on the shell of the nucleus, in the area of the projectile's impact. In the picture above, that would be nucleons #2 and 4 of the shell. Thus the Glauber model, due to its inherent simplicity, allows us to reduce a proton-nucleus interaction to a few proton-nucleon interactions, which are easier to calculate in QCD.

The Glauber model is often used as a reference in proton-nucleus and nucleus-nucleus collisions [5]. When the outcome of the interaction does not match the one expected from the Glauber model, more complicated interaction mechanisms are considered.

At high energy densities, one of these mechanisms currently discussed is the

formation of quark-gluon plasma. When energy density is sufficiently high, the QCD predicts formation of quark-gluon plasma [6] within the volume of the nucleus. This form of matter, like the atomic plasma, is characterized by the fact that the constituents lose their "host." In atomic plasma, electrons move from one ion to another, either binding themselves to an ion or continuing unbound movement. In quark-gluon plasma, an extended volume of interacting quarks and gluons is formed, with a size that is larger than the size of a hadron (typically around 1 fm) and temperatures exceeding some critical value estimated to be 180 MeV (10^{12} K). Though there are not much unambiguous experimental verifications of quark-gluon plasma's existence, there are calculations indicating that plasma formation is possible at energy densities of order of 1 GeV/fm^3 [5, 3, 6]. In heavy ion collision experiments at RHIC, this density has been achieved and overcome by a factor of ~10 [3], and the experimentalists have found evidence in favor of plasma formation. We note that, however, the high energy density is not the sole requirement for plasma formation.

Energy densities of order of 1 GeV/fm^3 are achieved at HERA-B, and the formation of plasma should not be discarded. The problem is that it is much more difficult to calculate theoretically the outcome of a p-A interaction according to the plasma formation model than according to the Glauber model. The interpretation of the results in the final state (i.e., the interaction products) is determined by the full time evolution of the colliding system [5], which includes several states, each of which is poorly known, even theoretically [3]. In particular, due to relatively poor understanding of the hadronization process, the final state does not tell us much about the initial process of the plasma generation, which makes backward extrapolation only approximate.

The conclusion of this discussion is that the plasma formation at HERA-B conditions is possible, and it may result in deviation from Glauber-model-based calculation of the phenomenon under study, in our case, of the A-dependence.

1.4. Mechanisms of Φ meson production in p-A collisions

It has been found experimentally, that different mesons have different production dependence on the atomic weight A, evidently due to different production and absorption mechanisms. In particular, in p-A collisions with J/Ψ and Υ heavy mesons in the final state, a strong suppression of these heavy mesons production has been observed [7]. (Suppression means that the production cross-section does not scale with the atomic weight A as quickly as in the case of other mesons.) The causes of this suppression are still unclear.

The production of the Φ which is the lightest bound state of strange quarks ($s\bar{s}$) is suppressed in ordinary hadronic interactions (i.e., in $q\bar{q}$ interactions) by the Okubo – Zweig – Iizuka rule (known as the "OZI rule") [8, 9]. Hence, the experimental studies of the Φ meson production details can shed some light on hadronic interactions taking place in p-A collision, such as the formation of the quark-gluon plasma or the absence of it.

There are theoretical calculations of the Φ mesons production in gg fusion which is thought to be the most probable mechanism of Φ meson production [8, 10]. In a gluon-gluon interaction, strange quarks and antiquarks are produced, leading to Φ meson

production. In a theoretical work [10], the Φ meson is thought to be produced in thermal equilibrium reached in the reaction zone, but the calculations have to be normalized to simultaneously produced J/Ψ meson in order to eliminate the unknown quantities.

In several p-p and p-A experiments certain aspects of Φ mesons production were studied, such as the ratio of Φ to K mesons [8, 11] and the increase of Φ meson production over pion production when heavier nuclei collide [12]. In general, the experiments confirm the g-g fusion mechanism of Φ production, which, in short, can be summarized with the formula: $g+g \rightarrow \Phi + X$. Not much more is known about the production mechanisms of the Φ or other mesons in nuclear matter.

1.5. The A-dependence of Φ meson production

The production of Φ mesons in inelastic high-energy p-A collisions, as well as the production of many other particles, depends on the atomic weight of the nucleus. The major factors determining this dependence are [8, 11-16]:

- The total inelastic cross-section of p-A interaction, which varies approximately as $\sigma_{total} \propto A^{\approx 0.7}$ (at HERA-B energies).
- The "exposed" area of the nucleus, where the major part of the interaction occurs, varies as $A^{2/3}$.
- The average propagation length through the nucleus, once the particle has been created on the surface of the nucleus, which varies as $A^{1/3}$. During this propagation, the

meson may be absorbed, or new mesons may be created by the products of the initial interaction.

The A-dependence as well as other aspects of the production can be experimentally studied. Virtually all experimental investigations parametrize the A-dependence of hadron production as a power law:

$$\sigma = \sigma_0 A^{\alpha} \qquad (1)$$

There are no theoretical grounds for this particular choice other than the simple facts listed above. The power law parametrization has another advantage: there is only one parameter describing the A-dependence. We will use this form as well.

Theories of A-dependence of meson production put forward several mechanisms, three of which we describe briefly below.

- Nuclear absorption:

  The strange fragmentation quarks are absorbed in the nuclear matter, forming other particles rather than an $s\bar{s}$ pair. The supposed mechanism, which is often used to describe nuclear absorption, is the following [17]. In the primary interaction, s and $\bar{s}$ quarks are formed. They capture a gluon from the interaction region and form a particle-like structure, which could exit the nucleus or its fragments and become a free Φ meson. But before the "pre-Φ meson" exits the nucleus, it has to travel through dense nuclear medium. Here the captured gluon has high probability to interact with a hadron of the original nucleus and disappear, thus breaking the bond between the s and $\bar{s}$ quarks. Each of them now hadronizes by itself binding other hadrons, and the

Φ meson finally is not formed.

- Comover absorption:

  The already formed pair interacts with secondary comoving hadrons, and is dissociated before it leaves the nucleus or the interaction region.

- Multiple scattering:

  The fragmentation quarks undergo scattering in the nuclear media, which hinders formation of $q_a\overline{q_a}$ pairs. $q_a\overline{q_b}$ pairs are formed with higher probability, since for a given flavor a there is a higher chance to encounter and bind to a flavor other than a because of the dominance of non- a flavors in the medium.

The published theoretical work, however, is not directly usable for comparison against the experimental results.

Chapter 2. The HERA-B experiment at DESY

2.1. The HERA accelerator ring

The accelerator HERA (German acronym for Hadron-Elektron Ring Anlage) is the main particle accelerator at DESY (Deutsches Elektronen-Synchrotron). HERA is a proton synchrotron, using both superconducting and ordinary magnets. It accelerates protons from other pre-accelerator rings.

HERA was built from 1984 to 1990, and put into operation in 1992. Until 2001, the energy of the proton beam was 820 GeV. During the accelerator upgrade in 2001-2003, the proton energy was increased to 920 GeV. The accelerator's infrastructure (tunnel, magnets etc) is used also for an electron accelerator with beam energy around 30 GeV. The accelerated electrons are not used in HERA-B, and the electron beampipe passes through the magnet and subdetectors of HERA-B with minimal distortion to the electrons' trajectories.

Protons are injected into the HERA ring after being generated through ionization of hydrogen and pre-acceleration by a liner accelerator, a small cyclotron and a smaller accelerator ring. Electrons undergo a similar path. Fig. 3 shows the accelerator chains.

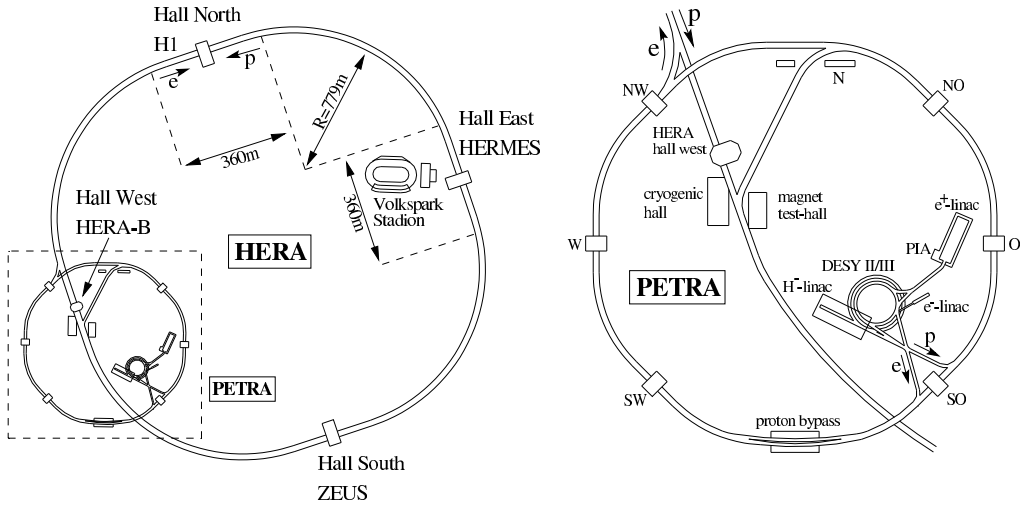

Fig. 3. Accelerator chains at DESY.

The proton beam consists of 220 buckets, of which only 180 are filled. There are typically 10^{11} protons in a filled bucket (bunch). The travel time around the ring is 21 μs, and the bunch crossing period is 96 ns. (The sequence of bunches has some other time structures which are not relevant here.)

2.2. The HERA-B experiment

The HERA-B experiment, located at the West Hall of HERA, was designed and built to study the CP violation of the so-called "golden decay" $B_d^0 \to J/\Psi \; K_s^0$ which is expected to have relatively strong CP asymmetry and well-detectable signature in the experiment. The first order Feynman diagram of the golden decay is shown in Fig. 4.

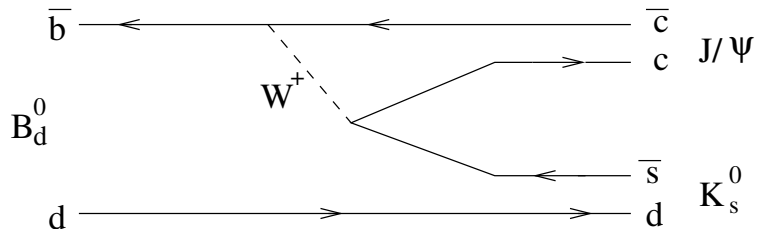

Fig. 4. The Feynman diagram of the golden decay.

The hardware of the HERA-B experiment was constructed to achieve this goal. See Fig. 5 for the drawing of the HERA-B spectrometer.

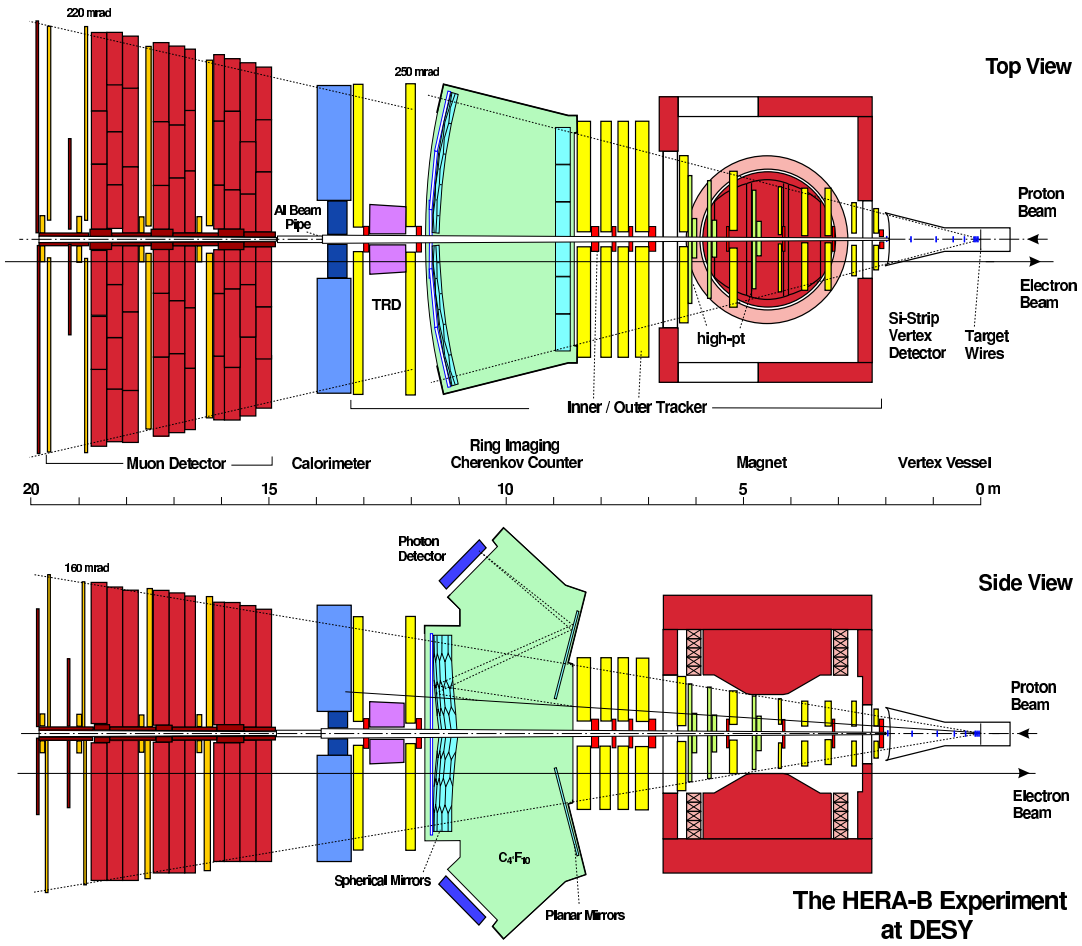

Fig. 5. Drawings of the HERA-B spectrometer.

Thin wire targets were placed in the halo of the proton beam, which do not deplete the beam. Protons interact with target material and produce many particles, usually order of 5-80. The long-lived ones are reconstructed by the silicon vertex detector, outer tracker and other components of the tracking system. The Ring Imaging Cherenkov detector allows the identification of pions, koans, protons, and to some extent electrons and muons. The electromagnetic calorimeter detects neutral particles (mostly photons), electrons and positrons. The muon detector detects muons that pass through the thick

calorimeter. The data acquisition system reads out the data from the detector, and, combined with the trigger decision, records the event data on magnetic tapes.

The hardware and software of the trigger system selects the events of interest, discarding the majority of uninteresting events. The software reconstructs the tracks from the hits in detectors, allowing the study of the p-A interactions. The HERA-B spectrometer is one of the most powerful and versatile detectors in the world.

Due to a number of difficulties, the main goal of the experiment could not be achieved. However, the spectrometer was used for several other studies [18-20], including this one.

The main components of the detector relevant to this study are:

- The wire targets.
- The silicon vertex detector.
- The outer tracker.
- The ring imaging Cherenkov detector.
- The trigger.

In the following sections of this chapter we will briefly describe the important aspects of the HERA-B detector, the process of data acquisition and analysis.

2.3. The targets of the HERA-B

The target system of the HERA-B is one of the most original and successful parts of the hardware. During the planning stage, it was realized that the luminosity of HERA is

more than enough for HERA-B. So, only a small fraction of the protons in the beam is needed for the experiment. There are three popular techniques known for utilization of a small portion of the luminosity of the beam in fixed target experiments: targets made of gas, ultra-thin foil and fixed wires. The last two types of targets cannot be used at HERA.

One positive consequence of the usage of small fraction of the luminosity is that when HERA-B starts operation in the designed mode, the other three experiments on HERA ring as well as the beam lifetime are not affected by its operation. Later it became clear that introduction of HERA-B's targets into the beam increases slightly the background level of other experiments, still keeping it in acceptable limits. The beam lifetime was almost not affected.

The proponents of the experiment found, however, another possibility [14]: to use thin wire targets (parallelepipeds with sizes approximately 0.1x0.5 x30 mm^3 or cylinders with 0.05 mm diameter and 30 mm length) in the halo of the beam. The problem is that the beam drifts. To accommodate the beam movements, the targets were put on movable holders which move in the manner the beam moves. (The mechanical reaction time of the targets is around 0.1 s, which is adequate most of the time, though is not quick enough to accommodate quicker beam movements. However, that response time was enough for the purposes of the experiment.) Fig. 6 shows a target wire and its holder.

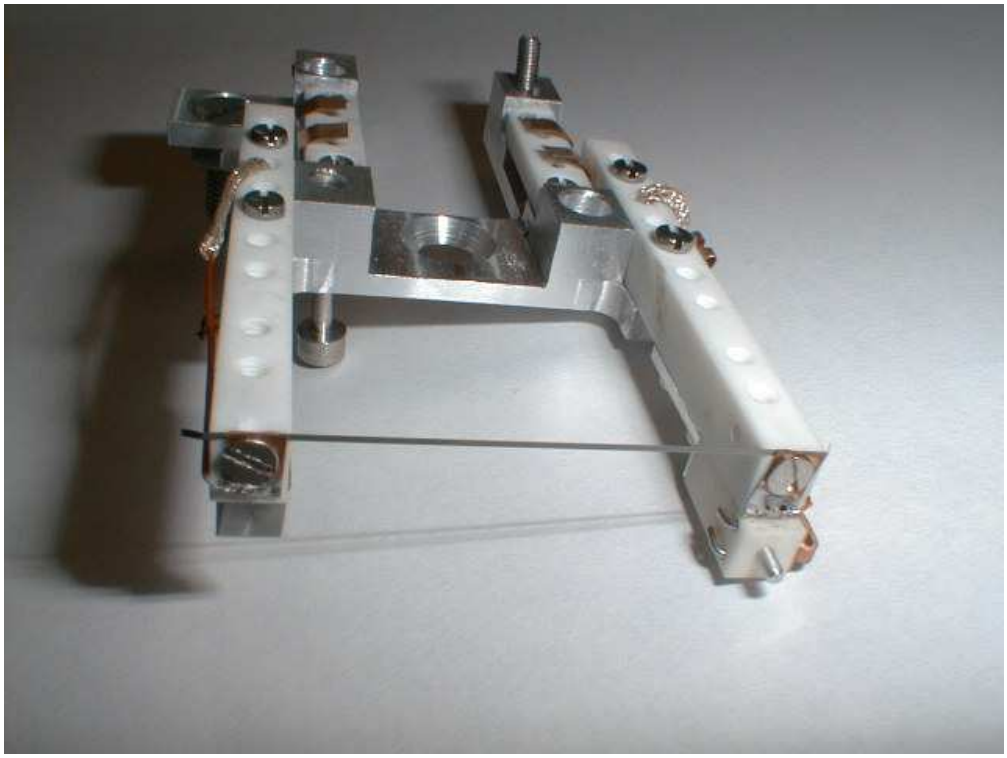

Fig. 6. A target wire on its holder.

Fig. 7 shows schematically the beam profile and two targets. Totally eight target wires were built, but in most cases 1-4 were used. Sometimes one of the wires was melted and broken apart, apparently because the high-intensity area of the beam crossed over the wire. These situations were automatically detected and at the nearest opportunity the wire was replaced.

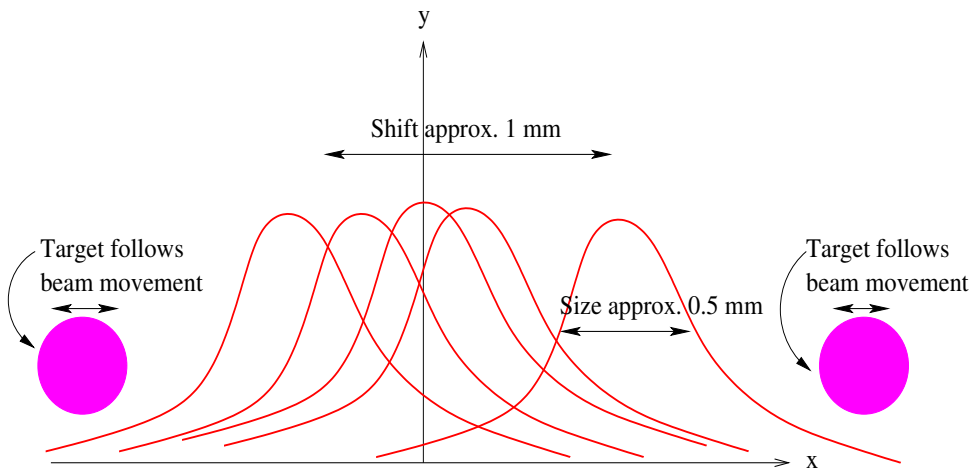

Fig. 7. HERA-B beam profile and two targets.

The eight targets were assembled in two stations approximately 4 cm apart. A target can move only along one direction perpendicular to its length: toward the beam or away from the beam. By utilizing special algorithms for target movements, desired interaction rate in a target is achieved and maintained during a run which lasts several hours. Fig. 8 shows the eight wires, their names and the coordinate system used at HERA-B and in this work.

HERA–B's targets and the coordinate system

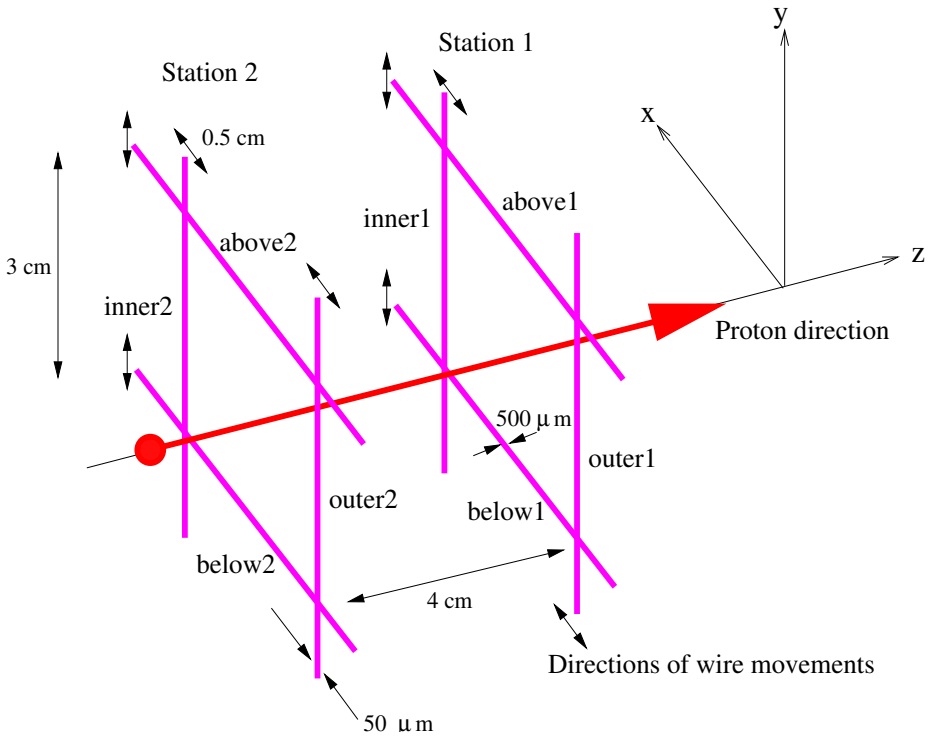

Fig. 8. The eight targets and the coordinate system.

Figures 9 and 10, taken from HERA-B history database, show the latitudinal positions of wires and the interaction rate achieved during a run. In Fig. 9, one can see that most of the time only one target, called inner 2, was active. On the interaction rate history, several spikes are visible. They indicate the moments when the target could not follow the quick movements of the beam. These spikes did not damage the particle detectors of the spectrometer.

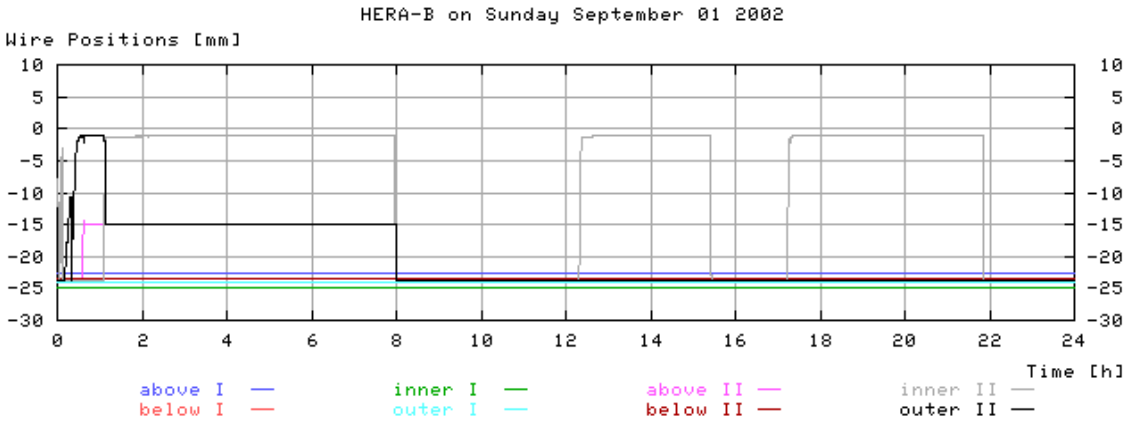

Fig. 9. Latitudinal positions of the targets (distance from the nominal center of the beam) during a run.

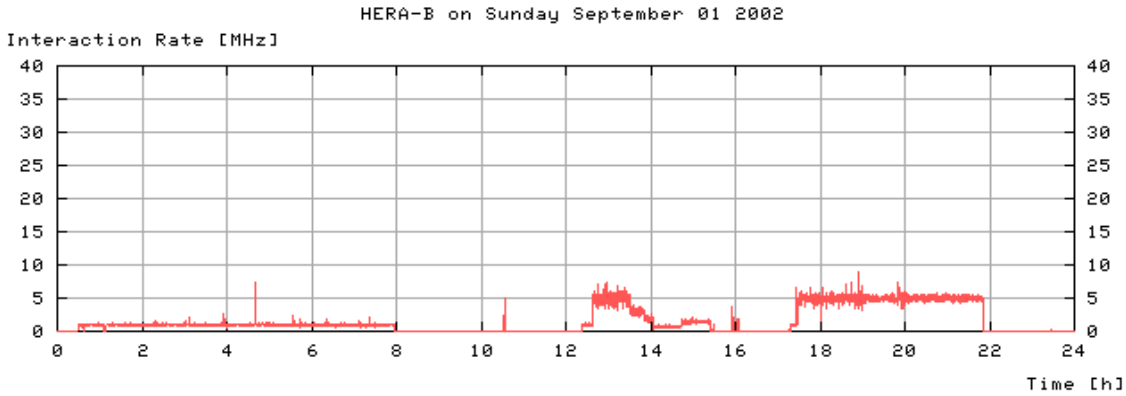

Fig. 10. Interaction rates (in MHz) during a run.

The target information (materials, positions, activity, calibration and alignment constants etc.) was saved in the run database and was used in this work.

2.4. The silicon vertex detector

The silicon vertex detector (SVD) is positioned between the target and the magnet. The task of the detector is accurate reconstruction of the tracks' segments, which is important for analysis of events occurring near the primary vertex. The detector contains 8 superlayers of silicon surrounding the beampipe, and has full angular acceptance excluding the beampipe (see the drawing in Fig. 11).

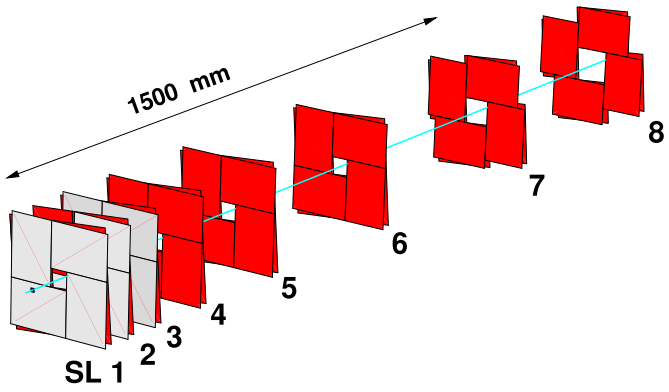

Fig. 11. Superlayers (planes) of the SVD.

The main challenge for the SVD was the high particle flux at the detector, leading potentially to quick aging of the silicon strips and the readout chips. Close to the beampipe, the flux is $3*10^7$ particles / ($cm^2 * s$). However, after 1 year of operation no aging was seen.

The detector provides high-resolution track reconstruction based on the large number of channels (around 150,000) and 50 μm readout pitch. The total length (along beam direction) of the detector is close to 2 m. See the photos in Figures 12 and 13.

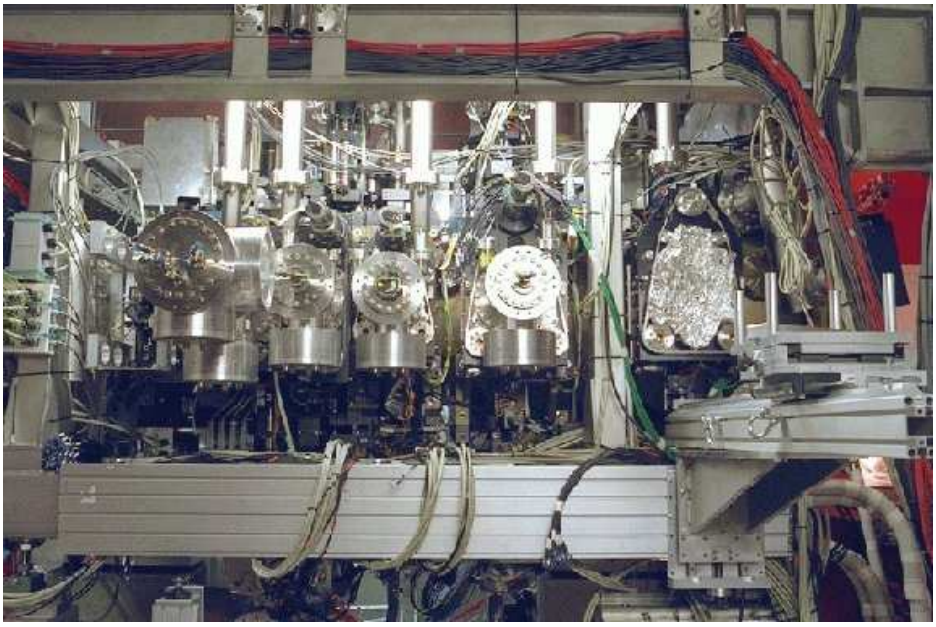

Fig. 12. Photo of the silicon vertex detector vessel.

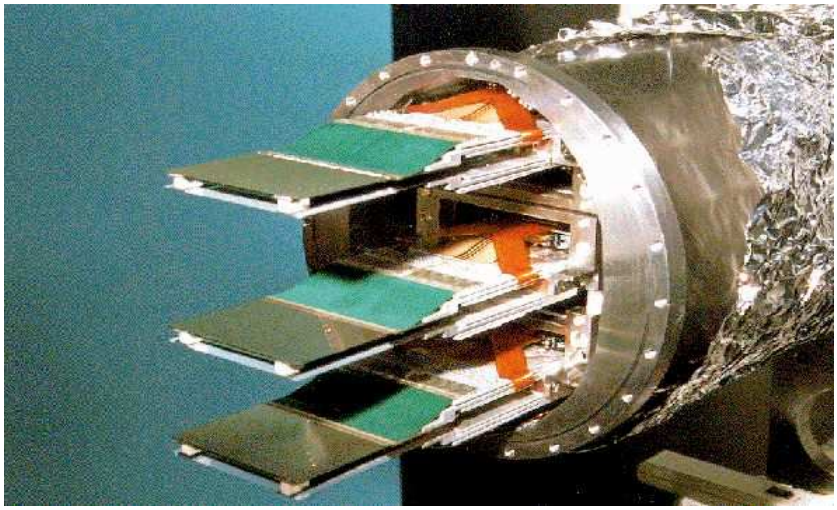

Fig. 13. Modules of the SVD.

The main achieved parameters of the detector are:

- Angular acceptance 10 – 250 mrad, which allows independent track reconstruction.
- Detector efficiency 97 – 99%.
- Track reconstruction accuracy: 500 μm along flight direction and around 25 μm in the

transverse direction.

- Multiple scattering and thermal expansion effects are the ones that limit the accuracy. The deviation of a hit at the rear superlayer due to multiple scattering is estimated to be 10 μm.
- The standalone track reconstruction, which is not a final reconstruction, provides, in typical cases, 95% track reconstruction efficiency, 6% ghost rate and 3% clone rate.

2.5. The outer tracker

The outer tracker (OTR) provides tracking inside the magnet and downstream up to the calorimeter. Geometrically, its parts are organized in superlayers similar to the SVD, but the size of each is much larger.

The OTR consists of hexagonal drift tubes, which use common gold-plated cathode and gold-plated wire. The chambers are assembled in a layer; the layers are assembled in a superlayer (mostly three layers per superlayer), and superlayers are assembled in modules. It has 120,000 channels. See Fig. 14 for the chamber design.

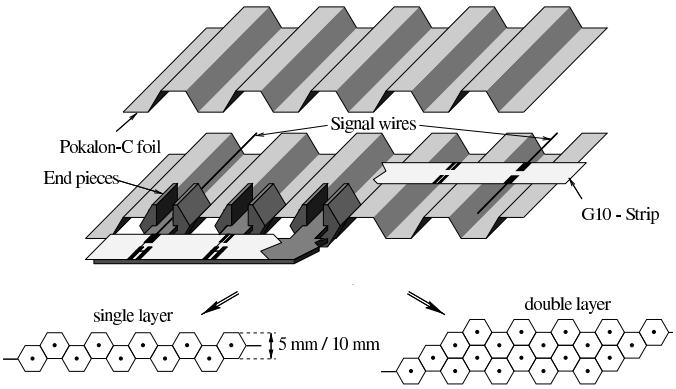

Fig. 14. The chambers of the outer tracker.

The main challenge of the design and construction lies in the large size of the OTR modules (the largest has sizes approximately 0.3 x 4 x 4.5 m^3) and quick aging of the straw chambers. After a series of aging tests, a design was found that survived the rate around 0.6 C/(cm*year). The gas mixture consists of 30% CF_4, 65% Ar and 5% CO_2.

Fig. 15 shows a module of OTR during installation.

Fig. 15. One of the modules of OTR during installation.

The main parameters of the detector are:

- Diameter of the wires is 25 μm.
- Gas gain is 30,000.
- Occupancy is 10-20%.
- Cell size is 5 or 10 mm.
- Efficiency of a cell is 92 - 98%.
- Typical efficiency of track reconstruction is 85 – 96%.
- A charged track has mostly 20-80 hits in the whole OTR.

2.6. HERA-B triggers and data acquisition

In high energy physics experiments, the average rate of data generation is often much higher than what the data acquisition system can handle. In HERA-B, there are several hundred thousand channels to be read out in each event, and the events arrive in most cases at a rate of one per 96 ns. (The events are read out and stored in a pipeline, but they cannot be fully processed and saved.)

The triggering system of the experiment makes a quick decision, to determine if the read out data shall be saved, based mainly on the presence of certain required attributes in the event. The quick decision has to be taken in the time interval during which the read out data is temporarily stored in a pipeline. The decision is obtained by reading out selected output from the subdetectors, like their occupancies, and by performing a partial reconstruction of the event.

The triggering system has several levels. When the data required for triggering arrive from one level to the next, the rate of event registration is decreased and the data size is increased.

The main levels of the triggering system are the following.

- **The pretriggers** have hardware logic. They inform the first level trigger (FLT) where to start the track search, or that certain conditions have occurred, e.g., a high-P_t track has been seen.
- **The FLT** trigger also has hardware logic, and can be tuned to certain types of events,

e.g., "two hit clusters detected in calorimeter ."

- **The second level trigger** (SLT) does the preliminary fast reconstruction of the event. This allows a quick decision to be taken whether the event shall be stored or not.
- **The fourth level** trigger is actually not a trigger, but rather an event selector, or an event "tagger." It performs a full and accurate reconstruction of events.

Table 2 summarizes the performance of the triggering system for most of the runs.

Table 2. The HERA-B trigger performance. Abbreviations: ITR = inner tracker, OTR = outer tracker; Muon = muon detector; SVD = silicon vertex detector.

Trigger type	***Input event rate***	***Re-duction factor***	***Subdetectors used***	***Channel numbers used***	***Decision time***	***Output rate***
FLT + pretriggers	10 MHz	200	ITR, OTR, Muon	150000	Less than 12 μs	50 kHz
SLT	50 KHz	100	SVD, ITR, OTR, Muon	400000	3.8 ms	500 Hz
Fourth level trigger	500 Hz	50	All	520000	4 s	25-50 Hz

Several trigger types were used: single lepton trigger, dimuon trigger, dilepton trigger, minimum bias trigger, interaction trigger, calorimeter pretrigger only, muon pretrigger only and others.

The main hardware components of the trigger are track finding units (around 70 printed boards) with lots of computing power on the boards, track parameter units (3), a trigger decision unit, a PC farm with 40 PCs, electrical cables and optical links. Photos of the boards and the FLT assembly are shown in Fig. 16.

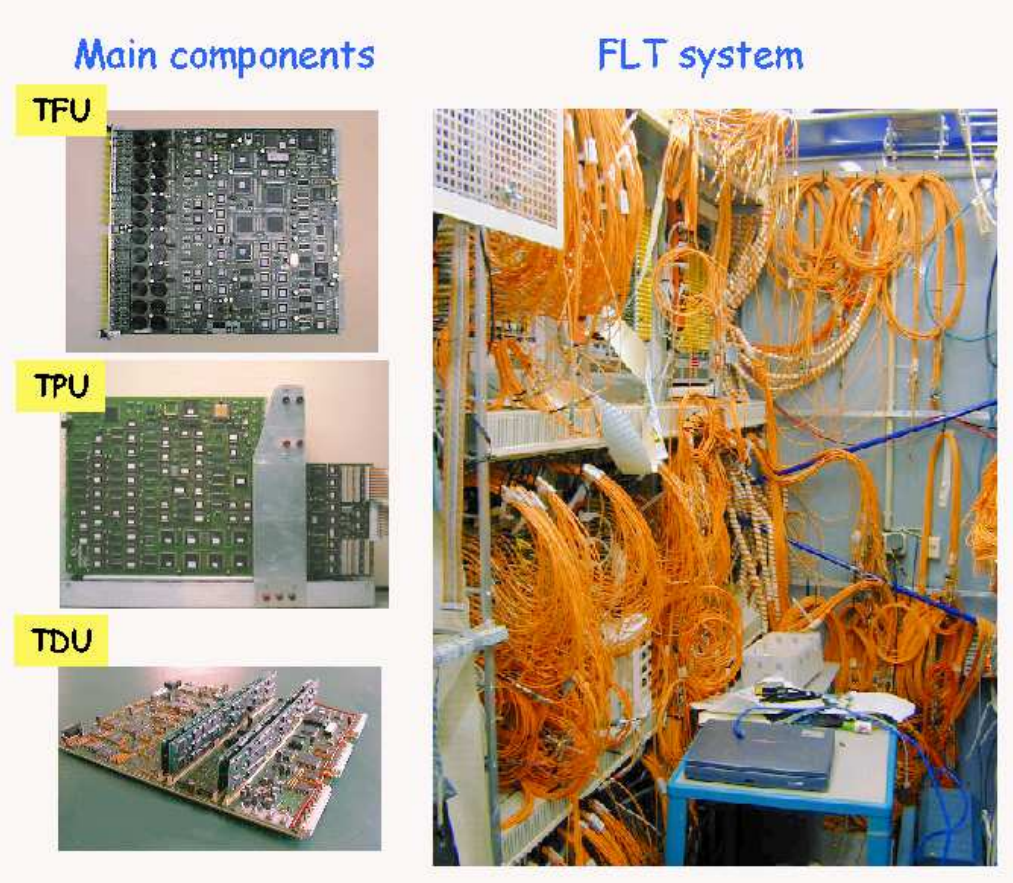

Fig. 16. Photos of the HERA-B trigger components.

The data acquisition system (DAQ) reads out the detectors once the trigger decision is positive. The steps of full data acquisition and reconstruction are:

- Read out data in the detectors.
- Store the data temporarily in a file, or reconstruct preliminary online with saving of the resulting files.
- Reconstruct fully later using the database of alignments, thresholds etc.
- Make the data containing the four-vectors and IDs of tracks (so-called mini files)

available for users.

- The subdetector experts then fill the databases for a full reconstruction that will be done later and with higher quality.
- If required, reprocess the data off-line one or more times, refining the procedures and constants iteratively. This step takes months to finish.

Users (the physicists) analyze the data usually in two steps: (1) by preliminary scanning for interesting events and saving them, and (2) by refining their analysis in the second step. Step 1 takes the major computer time. These steps are iteratively repeated. Fig. 17 shows usual data paths.

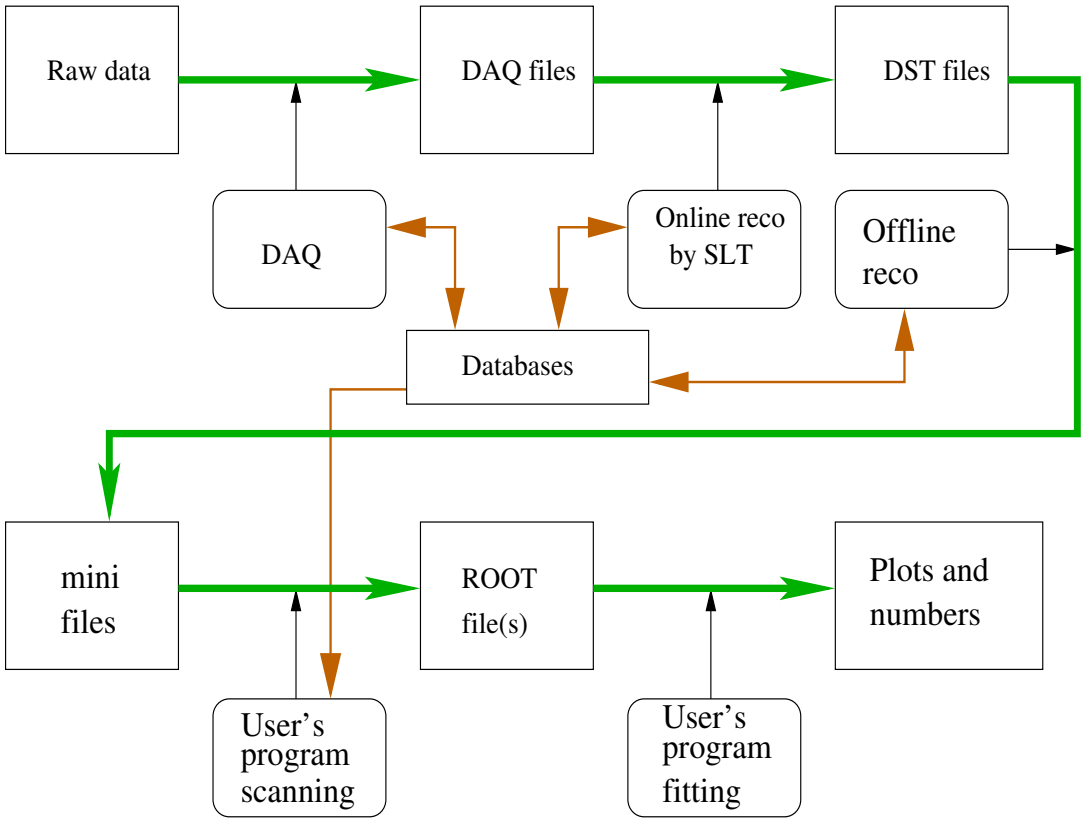

Fig. 17. The data flow diagram.

Chapter 3. The Ring Imaging Cherenkov detector and particle identification

3.1. Operation principle and particle identification with RICH

When a charged particle passes through a dielectric medium of refractive index n with a speed higher than the speed of light in the medium, it emits a cone of photons, called Cherenkov radiation. Since its discovery, Cherenkov radiation has been studied thoroughly both theoretically and experimentally. Today, enough is known about it to design and build detectors utilizing the effect [21]. We mention here the following important properties of Cherenkov radiation and its usage.

- The photons are emitted at a certain angle:

$$\theta_C = \arccos\left(\frac{1}{\beta n}\right) \qquad (2)$$

azimuthally symmetric around the trajectory. Here, θ_C (called the Cherenkov angle) is the angle between the photon's propagation direction and the trajectory of the charged particle and $\beta = v/c$ is the velocity of the particle. Hence, if one collects those photons with a lens or mirror, they will create a ring on the focal plane [21]. These detectors got the name "Ring Imaging Cherenkov Detector", or RICH. See Fig. 18 for the geometry.

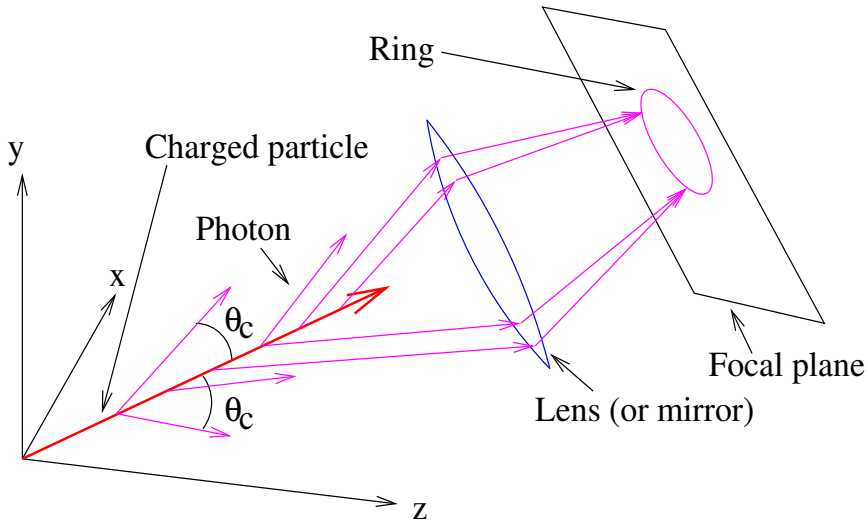

Fig. 18. Schematics of Cherenkov radiation and of ring formation.

- The spectrum of the emission is uniform in photon energy; hence, it scales as λ^{-2} in wavelength. Actually, there is a limit in the short wavelength edge, but it is not important for most of Cherenkov detectors. There is a well-known formula for the number of photons produced per unit length of the trajectory per unit wavelength interval [22]:

$$\frac{d^2N}{dx\,d\lambda} = \frac{2\pi\alpha z^2}{\lambda^2}\left(1 - \frac{1}{\beta^2 n^2(\lambda)}\right) \tag{3}$$

  Here N is the number of photons, α is the fine structure constant, z is the charge of the particle in units of electron charge. The absorption and scattering in the medium affects the spectrum of light arriving at the photon detector.

- In most cases, the usable spectral interval of the photons lies between near UV and visible. The absolute number of photons in most cases is not high, and one does not speak about abundance of photons. The number of photons per ring, N_{photon}, is a

critical parameter of the detector. It is often written as $N_{photon} = N_0 L \sin^2 \theta_C$, where N_0 is a constant depending on hardware, and L is the length of the radiator, 2.8 m for HERA-B RICH. In the HERA-B RICH, there are about 32 photons per ring [23].

- The Cherenkov angle θ_C is not a constant. It depends on the dispersion of light $n(\lambda)$ in the medium. Dispersion results in the broadening of the angular spectrum of the Cherenkov photons and smearing of rings.

Photons originated at the tracks of charged particles create rings on the focal plane which coincides with the entry plane of the photon detector. The Cherenkov detector records the rings - identifies them and finds the center and the radius. The Cherenkov angle can be found, to the paraxial approximation, by means of the formula $R = F\theta_C$, where F is the focal length of the imaging system (lens or spherical mirror). Once θ_C for a particle's track is found, its velocity is obtained from (2) assuming n is known. The tracking system of the spectrometer determines the momentum $p = \frac{m\beta}{\sqrt{1-\beta^2}}$ of the track. Now from this equation m - the mass of the particle - can be found, which is related to its ID. The track's charge is obtained from tracking. In small-angle approximation [24], the formula for mass is: $\theta_C = \theta_0 - m^2/p^2$, where θ_0 is the Cherenkov angle for saturated ($\beta = 1$) tracks.

Since the speed of the particle must be higher than certain value in order for Cherenkov radiation to occur, there are no rings formed if the particle's momentum is

below a certain threshold, which can be derived from the requirement $\beta > 1/n$. For particles with $\beta \approx 1$ the Cherenkov angle does not depend on β and saturation occurs. Both of these phenomena limit the resolution and the operating range of the RICH detector.

According to Fig. 18, we note the following property of the RICH detector: the position of the center of the ring depends on the direction of the particle's trajectory only. A parallel shift of the trajectory does not affect, to the first approximation, the position of the center of the ring. This creates an additional difficulty when tracks from tracking system are matched to tracks (rings) reported by the RICH.

3.2. Hardware design

The design must accommodate several requirements of the experiment. In HERA-B, like in other experiments, the main requirements are: the detector must have small radiation length (the RICH detector of HERA-B accounts for 20% of the total radiation length excluding the muon detector and calorimeter); the detector must serve its purpose of identifying charged particles; and there might be special requirements, which in HERA-B are: distinguish between kaons and pions up to momenta approximately equal to 50 GeV.

The choice of the medium for light generation and the geometry of the detector are the most important factors in the final design.

One would like to have large refractive index to get the maximum number of

photons per ring and large values of Cherenkov angle. However, with known materials, this would lead to large radiation length and large dispersion. Currently, heavy gases and aerogels are the main choice. The HERA-B RICH uses perfluorobutane (C_4F_{10}), which has a large refractive index of 1.00153 and low dispersion ($dn/d\lambda \approx 2.5 * 10^{-7} nm^{-1}$).

To collect and image the photons, HERA-B RICH uses two sets of mirrors. The first set consists of 80 spherical mirrors, which together constitute one spherical mirror cut into two pieces, each of which is slightly tilted with respect to the beampipe. The second set consists of 36 planar mirrors, which together constitute one planar mirror cut into two halves. The cutting of the spherical mirror into two tilted pieces reduces the total size of the detector, although it slightly increases the optical aberration [25]. The spherical mirrors are in, and the planar ones are out of the spectrometer acceptance. See Fig. 19 for the drawing of the RICH detector.

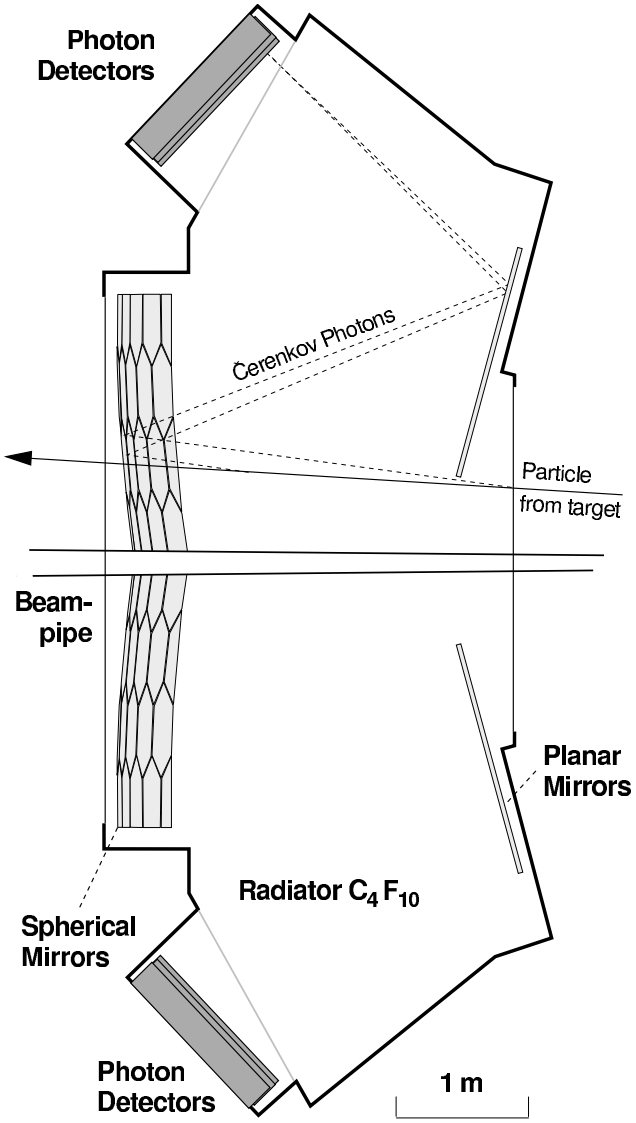

Fig. 19. The RICH detector.

Besides the gas system and the mirrors, the other major parts of the RICH are the photon detector and the readout system. We will describe here the photon detector only. As seen in Fig. 19, the photon detector consists of the upper and lower halves. The

photons are actually detected by an array of multichannel photomultipliers. Since the photosensitive area of the photomultipliers does not cover the whole image area because of gaps between the photomultiplier tubes, a set of lens telescopes reduces the image piecewise to project photons on the sensitive areas of the photomultiplier tubes only. Fig. 20 shows schematically a photon detector module. The outer surface of the field lenses is the surface on which the mirrors image the rings. The central region of the photon detector is covered with 16-channel photomultiplier tubes, meanwhile the peripheral region is covered with 4-channel tubes resulting in 4 times less channel density in peripheral region.

Simulations show that a cylindrical surface of the photon detector fits the focal surface better than a flat or spherical one. For this reason, the photon detector is divided into several flat-surfaced modules, which are tilted with respect to each other to approximate a cylindrical surface.

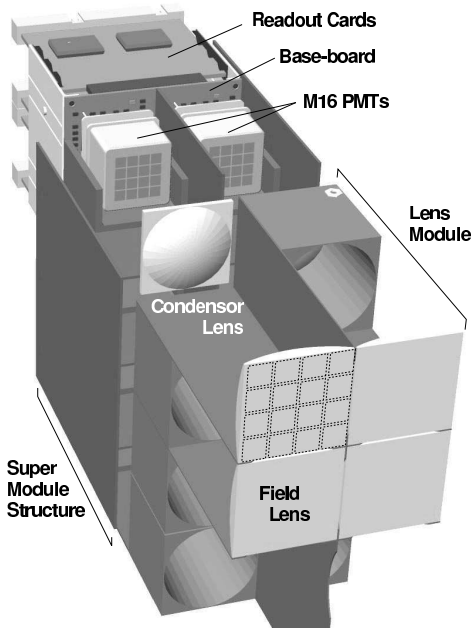

Fig. 20. The modules of the photon detector.

The following numbers characterize the overall performance and properties of the detector. In total, there are around 28000 channels. Sizes of photosensitive areas of one channel of the photomultiplier tubes are 4x4 mm^2 or 8x8 mm^2. Cherenkov angle for saturated tracks is 52 mrad. Spectral sensitivity lies in the range from 300 to 560 nm. Saturated rings have a radius equal to 30 cm on the entry plane of the photon detector.

3.3. Ring reconstruction algorithms

The task of the identification of rings in the hit array of the RICH detector is a known challenge for all RICH detectors.

It is convenient to transform the (x, y, z) coordinates of single photon hits in the

detector to (λ, ϕ) angular plane, where λ is the elevation angle of the photon (angle between the photon's trajectory and the (x, z) plane) and Φ is the angle between the trajectory and the (z, y) plane [26]. An illustration of the hits in this angular space is shown in Fig. 21, together with reconstructed rings.

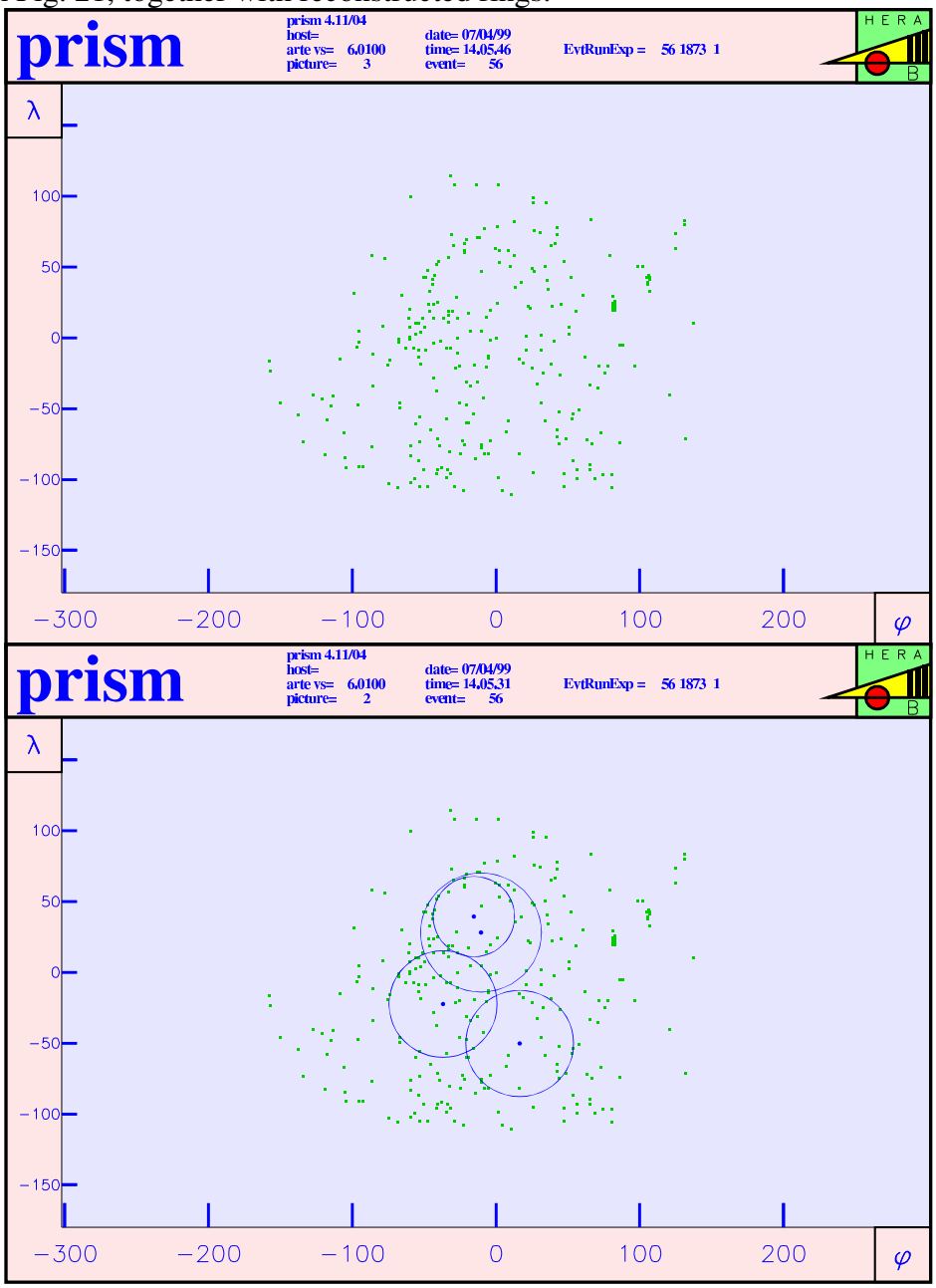

Fig. 21. An example of a sparsely populated RICH event with the hits (top) and the reconstructed rings (bottom).

There are several known approaches to the ring reconstruction problem.

The simplest approach uses information from the tracking system. Once a track is reconstructed without using the RICH information, even without an "ID", its (λ, ϕ) angles are known. Taking them as ($\lambda_{center}, \phi_{center}$) of the center of a potential ring, we can perform a ring search by drawing a series of concentric annular rings with thickness and step size approximately equal to the expected resolution. The annular ring that has (a) maximal number of hits and (b) for which that number is close to the expected value is declared to be the reconstructed ring. This algorithm is simple and robust. However, it is not used in the HERA-B RICH mainly because it relies on the reconstructed tracks.

The other group of algorithms performs a stand-alone ring reconstruction, without track angles from the tracking system. The obtained ring centers are then combined with the track information to yield the tracks and associate a Cherenkov angle to it if possible. The one used most often in HERA-B RICH is based on Hough's algorithm, which is illustrated in Fig. 22 [27] and can be briefly described as follows. Assume that a real ring (the thick ring in the middle) with radius R exists in a grid defined by the expected resolution. We define a reasonable search area for rings in the (λ, ϕ) angular space, taking all hit points in that area, using them as centers, and drawing rings with radius R . The two-dimensional histogram of intercepts (surface density of intercepts) of the drawn rings will then have a peak in the point where the center of the original ring is.

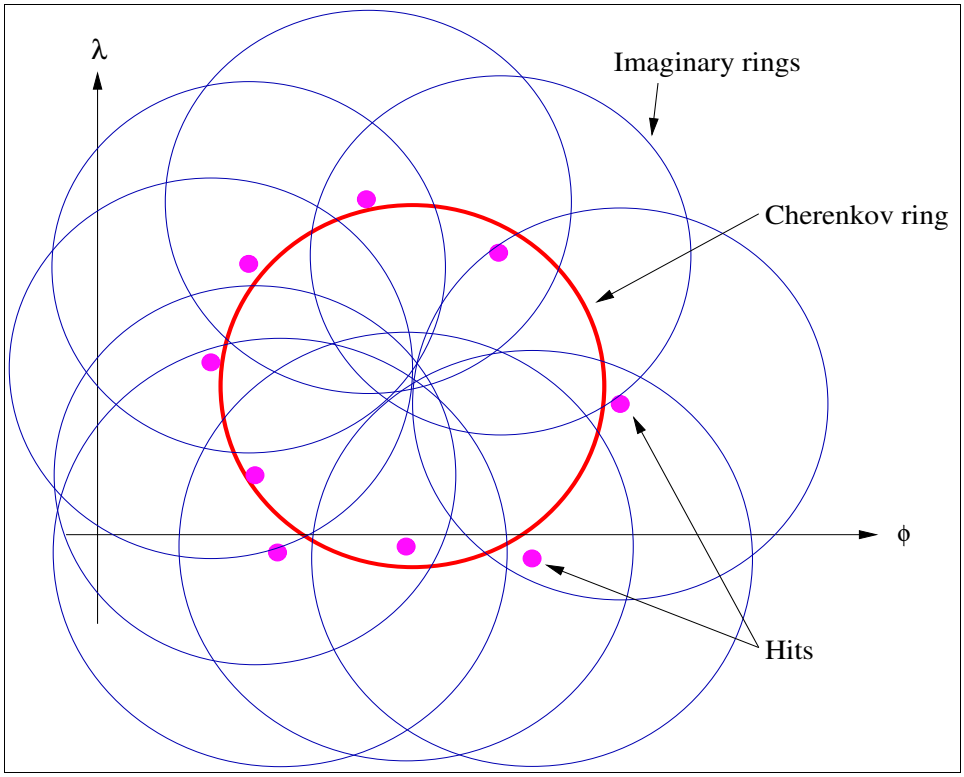

Fig. 22. The Hough algorithm for finding rings in a plane.

Of course, there are many issues in the algorithm: how to pick the radius; how is the angular grid size related to the photon detector cell size etc. But they can be solved by calculation, prediction or trial. In particular, the radius R is being tried descending from the radius of the saturated ring, which it is the most probable value.

Another approach is the so-called triangle-based algorithm [28]. Here, we use the fact that a ring is fully characterized by an inscribed triangle, from which it is easy to find the center and radius by a simple geometrical construction. Thus, any reasonable three-point combination of hits would give us a seed (more exactly a seed center and a seed radius) to start a ring search. A set of iterative mathematical procedures is then applied to

refine the center and radius by requiring minimization of χ^2 . Although this algorithm worked well, it is not used in HERA-B RICH since for medium- or densely-populated events the number of triangles is too high, and the algorithm takes an unacceptable large amount of CPU time.

One more approach develops the Hough's method further [29]. Once a ring candidate is found, we calculate the displacements of individual hits from the ring. Weights are assigned to the points based on the displacement: the closer the hit to the ring, the larger its weight. After every hit gets its weight, rings are recalculated based on the weights of the hits, and a new set of rings is obtained. The whole procedure is then repeated 1-3 times. It appears that the iterations quickly converge, yielding somewhat better ring parameters and particle IDs.

In actual HERA-B RICH ring reconstruction methods and programs, a large amount of refining considerations and corrections higher than the first order are used [24, 30, 31]. Here is a list of some of them, without calculations behind them.

- First- and partly second- and third-order optical aberrations due to large spherical mirrors are taken into account.
- It is possible to estimate the expected numbers of background hits as well as real photon hits in a cell and in an annular ring prior to reconstruction. This allows us to account for background hits during the ring reconstruction.
- A sophisticated logic is used to utilize the absence of hits in cells.

- Like most other subdetectors, RICH cannot reconstruct overpopulated events, which for HERA-B RICH means approximately more than 50-80 rings per event. In this case, the event is discarded.

3.4. Performance of the RICH detector

The main goal of the RICH detector is particle identification. The design required good separation between pions and kaons in the momentum range up to 50 GeV. This goal was achieved.

In the HERA-B RICH, the following particles are the important ones:

$\pi^{\pm}$, $K^{\pm}$, $e^{\pm}$, $p^{\pm}$, $\mu^{\pm}$. For identification purposes, for every type of charged particle there are three important values of momentum:

1) The threshold momentum, over which Cherenkov radiation begins. For kaons, the magnitude is equal to 9.6 GeV/c.
2) Ring reconstruction threshold, above which the reconstruction software gets enough hits (around 25) to reconstruct a ring in a real event where other rings are present.
3) The saturation momentum, above which the Cherenkov angle becomes practically indistinguishable from the saturated angle θ_0 .

In the (p, θ_C) plane a curve corresponds to each type of particle, and only a part of possible momentum range is useful for particle identification. In a real detector, naturally, there is smearing of points on (p, θ_C) plane, and the reconstructed points do

not sit exactly on the calculated curve. See Fig. 23, where the axes scales have been modified to yield straight lines for comparison with theoretical dependence.

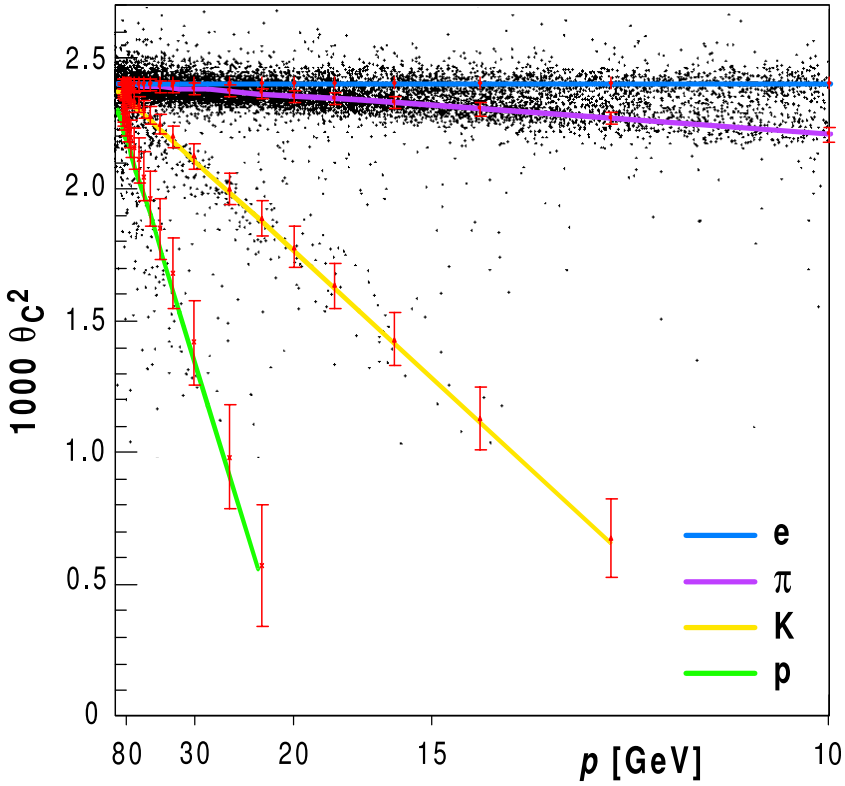

Fig. 23. Particles' Cherenkov angles versus momenta, for four most important particles. Points are experimentally obtained; lines are calculated dependence.

For particle identification, the determination of the Cherenkov angle is critical. The error the in determination of the ring's center is not critical as long as an association of a track and a ring can be accomplished. The radius error depends on the angular resolution of single photon hits. There are four important factors in determining the angular resolution of hits: angular size of a single photon detector cell, the dispersion in the

radiator gas, the optical imaging errors, and multiple scattering. Minor sources of background are the Rayleigh scattering in the gas and the electronic noise. Fluorescence in the gas and photomultiplier noise almost do not contribute to the error. Table 3 summarizes the contributions of the main factors to the single photon angular resolution for the central and the peripheral parts of the detector [23]:

Table 3. Single photon angular resolution in RICH.

Error source	***Central part***	***Peripheral part***
Angular size of the cell	0.5 mrad	0.93 mrad
Dispersion in the gas	0.33 mrad	
Optical errors	0.25 mrad	
Multiple scattering	$3.5\,mrad/p[GeV/c]$	
Total, added in quadrature for 20 GeV/c track	0.67 mrad	1.03 mrad

These numbers coincide with the experimentally observed values which were obtained by analyzing sparsely populated events with high momentum tracks (momentum around 50 GeV/c) of particles with known identity, e.g., muons from J/Ψ decays: the obtained single photon resolutions are 0.81 mrad for the central region and 1 mrad for the peripheral region [23]. Of course, Table 3 does not include all sources of errors for determination of single photon angular resolution. Not included are: electronic noise (channel crosstalk); variation of the refractive index of the gas; optical noise (scattered photons), the magnitude and effect of which is difficult to estimate.

From the single hit resolution, the ring radius error can be deduced. In the real detector, however, overlapping rings, varying refractive index of the radiator gas, intrinsic mechanisms of the ring reconstruction algorithm affect the radius, and the error

in radius determination is worse than $\frac{\sigma_{\text{single photon}}}{\sqrt{N}}$ [23]. The ring radius error for almost saturated pion tracks is estimated to be around 1 mrad [48].

Finally, Fig. 24 demonstrates π/K separation as a function of momentum. For this study, both Monte Carlo simulation and experimental methods were used to find out the ID of the track independent of RICH. The vertical axis shows pion and kaon hypothesis likelihoods.

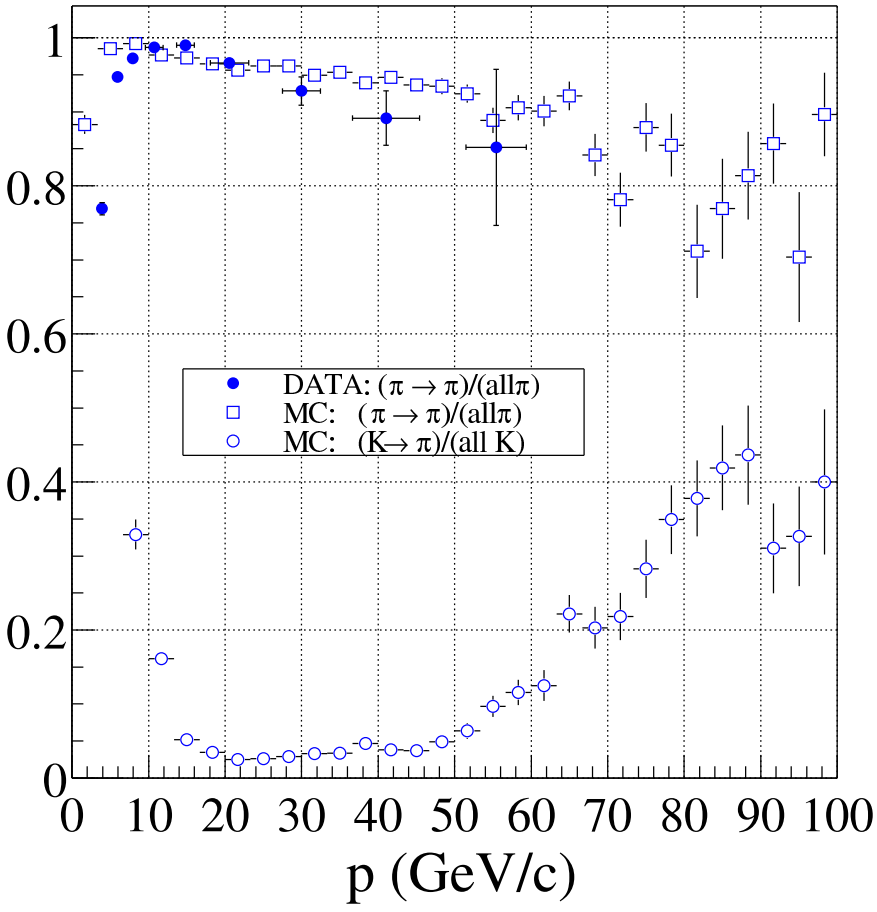

Fig. 24. Curves for pion/kaon separation obtained by Monte Carlo and experiment.

For normal users, the HERA-B reconstruction software provides particle likelihoods for tracks based on methods described in 3.1 and 3.3. Likelihood values are normalized to lie between 0 and 1. A track can have several particle likelihoods different from zero.

Usually the reconstruction of the ID is almost impossible for tracks whose momenta are only slightly above the threshold. A study was performed to find out the relative ratios of generated particle types [30, 32] . Based on this study, in the case when RICH cannot identify the particle, a likelihood is assigned to the track based on the hypothesis that the track is a pion with probability approximately 1/4, is a kaon with probability 1/5, and similar values for several other particles. Sometimes the data from other subdetectors help to improve this guess. For example, the muon detector can almost for sure identify muon tracks.

This work deals mostly with kaons and pions. Fig. 25 shows histograms of the RICH likelihood for those tracks that passed several preliminary criteria. Kaons and pions in the histograms have passed different cuts, which is the reason for the presence of the strong zero peak for pion likelihood histogram and the absence of a similar peak in kaons' histogram.

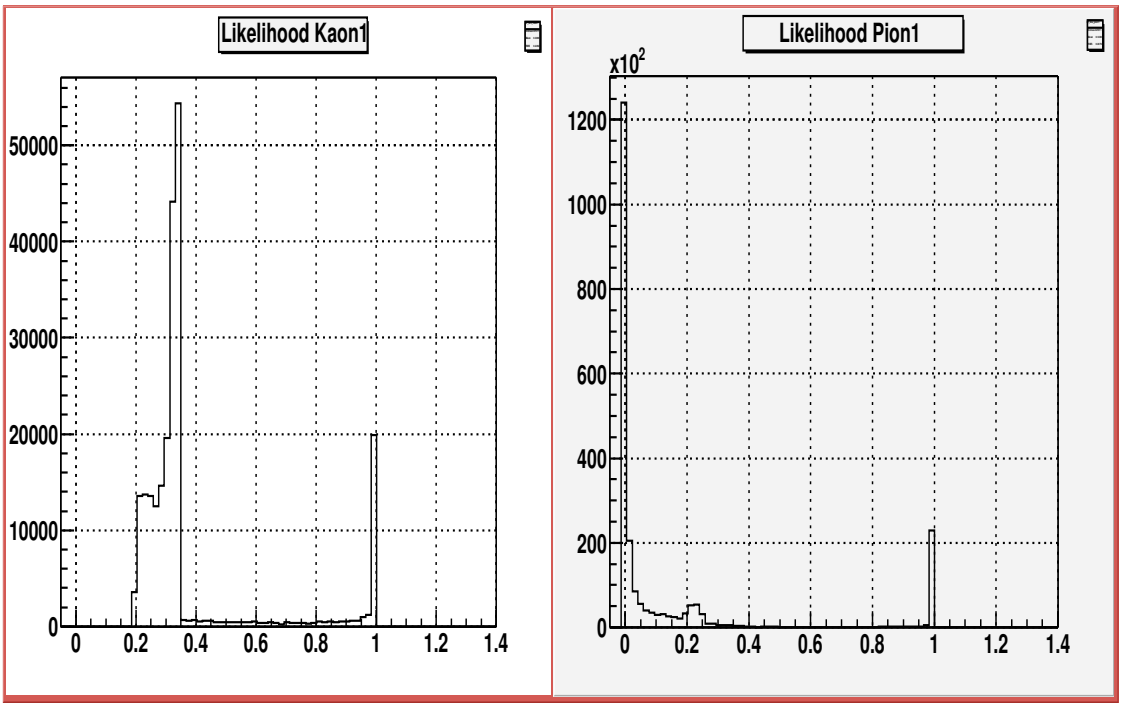

Fig. 25. Kaon and pion likelihoods from RICH after the tracks pass several cuts.

As the following chapters will show, the particle IDs obtained from RICH are sufficient for the purpose of this work. ID likelihoods from other subdetectors provided almost no improvement in kaon likelihood.

Chapter 4. Data analysis for obtaining the A-dependence

4.1. The data sample

Until now (winter of 2003), there were two data taking periods at HERA-B: in the summer-fall 2000 and in October 2002 - March 2003. The data sample taken in year 2000 is several times smaller than that in the 2002-2003 period, and currently is not used. The analysis performed in this work uses the data from the second data taking period.

The notion of a run is important in most accelerator experiments. The HERA accelerator works in cycles. Without going into details, one cycle includes the following stages: fill; acceleration; adjustments; luminosity run; and beam dump. The total duration of one cycle is approximately 10 hours, of which the luminosity run takes 1-8 hours. During the luminosity run, HERA-B and other experiments take their data in data taking runs, or, shortly, "runs." One run lasts from minutes to hours, during which usually several hundred thousand events are read out by the DAQ. Every data taking run has its unique number. Naturally, it has also a "run configuration", which includes the subdetectors used, their operating parameters, the trigger type, the target wires used, interaction rate and many other quantities. Some of them are not changing during the run, others vary, and the important ones are written into the database.

For the purpose of obtaining the A-dependence of the Φ production cross-section,

the trigger type appeared to be not important (see below), but we need runs with at least two active targets.

The following figures characterize the amount of data available. There were totally 521 million events taken. Of those, 472 million were reprocessed (i.e., the tracks were reconstructed). Some loss is due to over- and underpopulated events, software and hardware bugs, lost communication, hard drive crashes and other reasons. Out of the 472 million events, 123 million are of interest to us - others were mostly one-target runs and tests. Runs with three targets appeared to be bad and unusable. Runs with four targets have only 0.16 million events and are not useful. There were no runs taken with 5 or more active targets. Some runs were taken with no target wires, registering parasitic "beam gas" interactions.

The two main trigger types used were "interaction trigger" and "physics." The interaction trigger requires an inelastic event resulting in detectable tracks. The physics trigger, in addition, requires different properties of events and tracks suited for a particular physics goal, e.g. the presence of two or more muons for J/Ψ study. Almost all of the trigger types, including physics triggers, are suitable for our goal, and the data of those triggered events were used for obtaining the A-dependence.

The majority of runs with two targets were taken with carbon (C) and tungsten (W) wires. There are some runs with carbon-palladium (C-Pd) and carbon-titanium (C-Ti) wire combinations. There are many runs with C-C combination, from which the A-dependence cannot be derived, but are very useful for the estimation of the systematic error of $\Delta\alpha$. Table 4 summarizes the available numbers of events and target materials

used.

Table 4. Target materials and number of events.

Number of targets	***Number of useful events (million)***	***Materials and material combinations of the targets***	***Number of useful events with material combinations (million)***
0	0	Beam gas	Not important
1	326	C, W, Al, Ti, Pd, W+Re alloy	Not important
2	123	C-W	96
2		C-Ti	16
2		C-C	11
2		C-Pd	0.7
3	0	None	0
4	0	C, Al, W, Ti	0
5 - 8	0	None	0

4.2. Criteria for the selection of Φ mesons

The Φ meson generated in an inelastic p-A collision is not detected directly by the HERA-B spectrometer since it has a very short lifetime (full width at half maximum FWHM is 4.43 MeV and lifetime is $1.5*10^{-22}$ s). The estimated flight length is $c\tau\gamma \approx 10^{-12} m$ [22]. The selection of the Φ mesons has been done, as usual in high energy physics experiments, through their decay products. In 49% of the cases, the Φ meson decays into two charged kaons K^+ and K^- according to the Feynman diagram shown in Fig. 26.

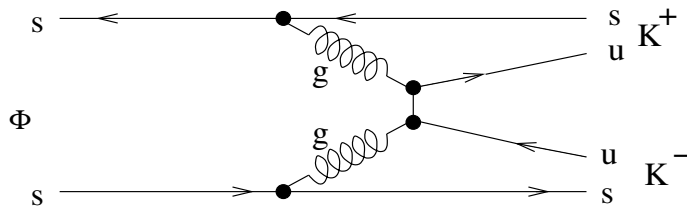

Fig. 26. The most probable Φ decay mode.

The kaons have long flight paths (several meters), and are detected by the spectrometer. We have the following:

1) The track is detected, and its ID is found (in this case, through RICH).

2) The momentum $\vec{p}$ before the magnet and the charge of the particle are obtained.

3) A point (x, y, z) on the track before the magnet is obtained.

This amount of information about tracks allows us to arrange kaons into pairs, calculate their invariant masses and to consider the pair as a decay product of a Φ meson. Of course, each of these quantities comes with some error or uncertainty. The main requirements for arranging kaons into pairs are that they originate from a single point and have opposite signs. The check against origination from a single point is done through the calculation of the distance of closest approach (DCA) of the two tracks in three-dimensional space, and by requiring that the DCA be small, order of transverse resolution of the spectrometer (estimated to be 0.2 mm). In reality the two tracks do not intersect, but approach each other up to some distance, equal to DCA. Excluding some unimportant special cases, there exists a unique shortest straight line segment, connecting the two tracks. The middle point of this line segment is called the DCA point, or the secondary vertex. The Φ meson, which was produced at the primary vertex, decays at the secondary vertex.

For the convenience of handling the large amount of data, the writing the program code, and the efficient use of computer time, the analysis is divided into two steps.

In the first step, called pre-selection, the data are scanned with weak cuts to find kaon candidates (a cut is a selection: if an entity does not satisfy the selection, it does not "survive the cut"). Other important cuts involved are the event quality cuts and track quality cuts. The full list of cuts will be shown below. The first step takes place at DESY. The user programs, created inside the HERA-B software framework called ARTE, run in one or several PCs at the DESY analysis farm. The outcome of this scanning is a ROOT file, which contains information about the events, selected pairs, their invariant masses, kaons likelihoods, geometry of tracks etc. The file is usually quite large, and many of those files have been created for this work.

In the second step the ROOT files are transferred to user's desktop PC. Another program, outside of ARTE, runs on the data in the file and applies stronger cuts and more refined logic to reveal the Φ mesons. (If the result obtained is unsatisfactory, the cuts or logic can be changed at the user's desktop PC, and the program is re-run.) The outcomes of the second step are a set of histograms, from which the results in this work are derived.

We use the following terms to characterize the geometry of targets, tracks and vertices. The distance along the z direction between the middle of the target and a secondary kaon-kaon vertex is called detachment from target. Since there are at most eight targets, each secondary vertex has eight detachments. The three-dimensional vector pointing from a primary vertex to a secondary vertex is called flight vector: along this

vector the mother particle is supposed to have flown. In reality, this vector in case of $\Phi \to K^+ K^-$ decay is so short that it is undetectable; however, the reconstruction software yields some nonzero length and a certain direction for it (possibly upstream), the length being approximately equal to the longitudinal resolution of the vertices $\Delta z \approx 0.7\, mm$. Due to this error, the histogram of Δz is almost symmetric around zero, from which we conclude that in this study we deal mostly with directly produced Φ mesons or with indirectly produced Φ mesons with flight length of the mother particle around 1 mm. However, the symmetry of the histogram indicates that the fraction of the latter ones is small. If a primary vertex can be assigned to a target wire, it is called a wire vertex. Fig. 27 below gives a schematic overview of the geometry.

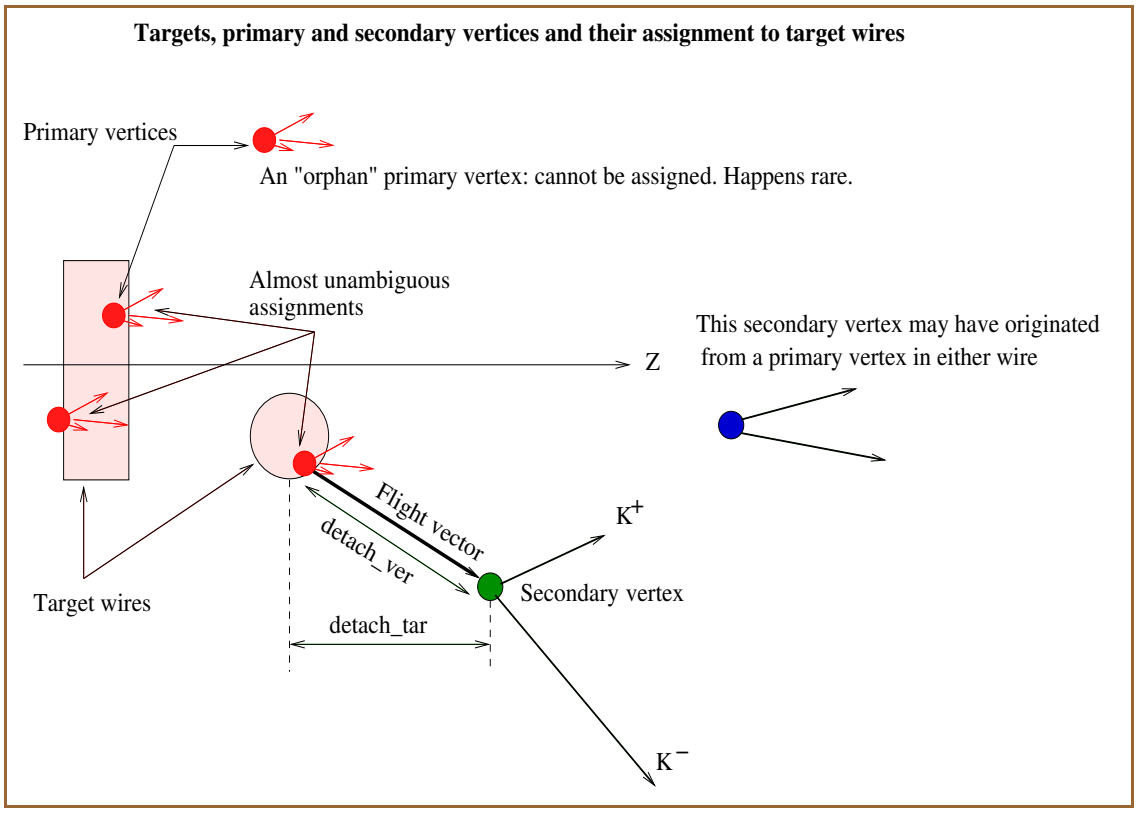

Fig. 27. A simplified picture of targets and vertices in HERA-B.

Once more, the major "physics" cuts are the particle likelihood, quality and kinematic cuts. Besides, a set of "technical" cuts are applied to ensure the safe running of the programs, an example of which is a requirement of the presence of the event's descriptor header in the reconstructed event.

The tables below show the cuts applied for Φ selection, and the survival rate. When estimating the total survival rate after application of several cuts, one shall not simply multiply the survival rates of individual cuts - the logic is more complicated.

The first group of cuts is applied during scanning:

1) Event quality cuts

NN	***Description***	***Expression, schematic***	***Estimated survival rate***
1	Event must contain a normal header (with date, run number etc)	EVHD	1.0
2	Table of reconstructed tracks must exist	RTRA	0.99
3	Table of reconstructed primary vertices must exist	RVER	0.95
4	Table of reconstructed targets must exist	GTAR	1.0
5	Occupancy high enough for two rings in RICH but not too high	N_hits_RICH between 40 and 3000	0.9
6	Primary vertices are from targets	vwv not empty	0.95
7	Take only the four strongest primary vertices, discard others	vwv.sort()	0.9
SUB-TOTAL			0.79

2) Track quality cuts

NN	*Description*	*Expression, schematic*	*Estimated survival rate*
1	Number of hits in SVD	N_SVD > 5	0.4
2	Number of hits in OTR	N_OTR > 10	0.6
3	Track is not neutral	RTRA != 6	1.0
SUB-TOTAL			0.24

3) Likelihood cuts

NN	*Description*	*Expression, schematic*	*Estimated survival rate*
1	Kaon likelihood of track 1	lk1 > 0.20	0.5
2	Kaon likelihood of track 2	lk2 > 0.20	0.5
SUB-TOTAL			0.25

4) Kinematic cuts

NN	*Description*	*Expression, schematic*	*Estimated survival rate*
1	DCA must be small	DCA < 2 mm	0.9
SUB-TOTAL			0.9

TOTAL AT DESY: Survival rate = 0.043.

The second group of cuts is applied at the user's desktop:

5) Track quality cuts

NN	*Description*	*Expression, schematic*	*Estimated survival rate*
1	Number of hits in SVD	N_SVD > 9	0.3
2	Number of hits in OTR	N_OTR > 22	0.4
SUB-TOTAL			0.12

6) Likelihood cuts

NN	*Description*	*Expression, schematic*	*Estimated survival rate*
1	Kaon likelihood of track 1	lk1 > 0.70	0.05
2	Kaon likelihood of track 2	lk2 > 0.70	0.05
SUB-TOTAL			0.0025

7) Kinematic cuts

NN	*Description*	*Expression, schematic*	*Estimated survival rate*
1	DCA must be small	DCA < 0.3 mm	0.6
2	Opening angle, to remove clones and bad pairs	Between 0.001 and 88.88 rad	0.99
3	Pair's mother's flight distance	detach_ver < 1 mm	0.95
4	Impact parameter	impact < 0.5 mm	0.7
SUB-TOTAL			0.39

Total at user's desktop: 0.00021.
Estimated cumulative survival rate: $9*10^{-5}$.

Thus only a small amount of events, tracks, and pairs survives the cuts, to yield an

invariant mass that might indicate that the pair of kaons selected was born in the decay of a Φ meson.

Once the invariant mass of the pair that survived the cuts lies under the phi peak, the particle from which the pair has originated is called a "Φ meson candidate", or, shortly, Φ - we do not have any more handles to differentiate between the Φ meson candidates and the actual Φ mesons. An example of a Φ peak is shown in Fig. 28.

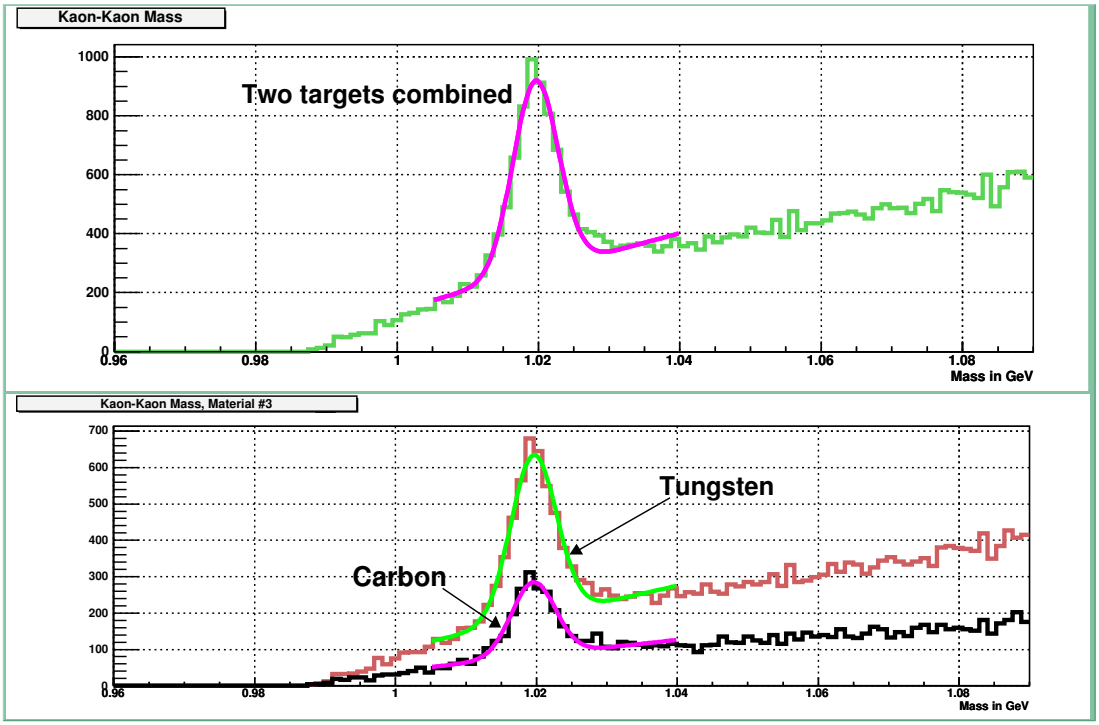

Fig. 28. The Φ peaks obtained. The upper picture shows the histogram of kaon-kaon invariant mass. The lower picture shows the same, divided into two targets: the histogram with more entries is for W wire and the one with less entries is for C wire.

The Φ mesons are then associated with target wires in two steps. First, the secondary vertex is associated with a primary vertex based on flight distance and impact parameter - both must be small. Second, the primary vertex is associated with a target wire through

the information in the experimental data. Thus, the target number and material where the Φ meson was produced become available, which allows the derivation of the A-dependence as described in the next section of this chapter. Almost every secondary vertex (more than 99%) can be associated with a target, so there is almost no loss of data because of target assignment .

4.3. Obtaining the A-dependence

Let us consider the case of two targets made of materials X and Y. Let us assume that, in a given run, where conditions and targets do not change, there are,

correspondingly, N_{inel}^{X} and N_{inel}^{Y} inelastic interactions in the targets.

Let us discuss the number of inelastic events and events with a Φ meson in final state on material X. Using a well-known formula for the number of events, we write:

$$N_{inel}^{X} = \sigma_{inel}^{X} \epsilon_{inel}^{X} L \ , \qquad (4)$$

where σ_{inel}^{X} is the inelastic cross-section for the p-A interaction, ϵ_{inel}^{X} is the efficiency of the event registration and L is the integrated luminosity. Assuming the conventional

A^{α} dependence of hadron production cross-section (1), we write: $\sigma_{inel}^{X} = \sigma_0 \left(A^{X}\right)^{\alpha}$,

where σ_0 is a constant and A^{X} is the atomic weight of the material X. With this, (4) becomes:

$$N_{inel}^{X}=\sigma_{0}(A^{X})^{\alpha}\epsilon_{inel}^{X}L \tag{5}$$

A similar consideration yields for the number of detected Φ mesons

$$N_{\Phi}^{X}=\sigma_{\Phi 0}(A^{X})^{\alpha_{\Phi}}\epsilon_{\Phi}^{X}L \tag{6}$$

where $\sigma_{\Phi 0}$ is a constant, α_{Φ} is a parameter characterizing the A-dependence of Φ meson production, ϵ_{Φ}^{X} is the detection efficiency for Φ mesons.

Dividing (6) by (5), we get the number of detected Φ mesons per inelastic interaction:

$$\frac{N_{\Phi}^{X}}{N_{inel}^{X}}=k\left(A^{X}\right)^{\Delta\alpha}\frac{\epsilon_{\Phi}^{X}}{\epsilon_{inel}^{X}} \tag{7}$$

where k is a constant and $\Delta\alpha=\alpha_{\Phi}-\alpha$ is the parameter characterizing the nuclear dependence of Φ meson production in an inelastic event. If $\Delta\alpha=0$, we say that there is no nuclear dependence, i.e., Φ mesons production cross-section and inelastic cross-section depend on A in the same way.

Writing the formula (7) for material Y and dividing the two formulas, we get:

$$\frac{N_{\Phi}^{Y}/N_{inel}^{Y}}{N_{\Phi}^{X}/N_{inel}^{X}}=\left(\frac{A^{Y}}{A^{X}}\right)^{\Delta\alpha}\frac{\epsilon_{\Phi}^{Y}}{\epsilon_{\Phi}^{X}}\frac{\epsilon_{inel}^{X}}{\epsilon_{inel}^{Y}} \tag{8}$$

There are two things to notice about (8). First, the integrated luminosity has been canceled out. Second, the ratio of efficiencies ϵ_{inel}^{X} and ϵ_{inel}^{Y} is close to 1 because of high number of tracks in an event (independent of material), which cause the trigger to fire; see Fig. 28. We introduce a quantity Q, called ratio of ratios, to be

$$Q = \frac{N_{\Phi}^{Y} / N_{inel}^{Y}}{N_{\Phi}^{X} / N_{inel}^{X}} \qquad (9)$$

With these, we finally obtain the formula for $\Delta\alpha$:

$$\Delta\alpha = \frac{\ln(Q) + \ln\left(\frac{\epsilon_{\Phi}^{X}}{\epsilon_{\Phi}^{Y}}\right)}{\ln\left(\frac{A^{Y}}{A^{X}}\right)} \qquad (10)$$

To find $\Delta\alpha$ according to (10), we need the absolute numbers of interactions for each of the materials occurred in a run or a set of runs. The number of interactions is not equal to the number of triggers, since in one trigger (i.e., for one recorded and reconstructed event, or simply in one "event") several interactions can occur in different parts of target wires. It is also possible, but irrelevant for this study, that during one bunch crossing no interaction occurs. These events are called empty events, and they were almost not recorded during the second data taking period.

We find the number of interactions in an event by looking at the primary vertices in that event. The HERA-B trigger in minimum bias mode detects more than 99% of inelastic interactions. We will assume that the number of interactions and the number of primary vertices are almost equal. Here are the considerations behind that statement. The HERA-B software package reconstructs primary vertices reliably once there are three or more charged tracks originating from a small volume, with sizes comparable to the longitudinal and latitudinal resolutions [33]. It is possible that there are one or two tracks originating from a primary vertex. In this case, we have a situation "an interaction

occurred but no vertex reconstructed", and counting the number of interactions through counting the number of primary vertices will result in underestimation. However, the number of those vertices is small compared to total number of vertices with three or more tracks, as shown in studies for the software package preparation [34] and in a small study done for this work, the histogram of number of tracks being shown in Fig. 29 after [34].

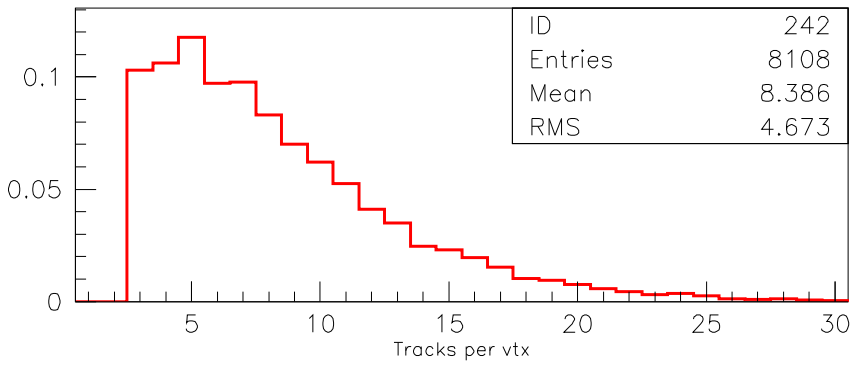

Fig. 29. Histogram of number of tracks from a primary vertex. Normalized.

Besides, the small error that will be introduced by underestimated counting will cancel out in the ratio in (9).

Thus we assume that the number of interactions and the number of primary vertices are equal. The latter can be experimentally measured.

Although not very important, a separate study was performed to find out the average number of interactions in a reconstructed event. It appears that the distribution is almost Poissonian, which is common in particle collisions, with the average number between 1 and 2. Fig. 30 shows the histogram and the Poissonian fit to the distribution for a short time interval in a particular two-target run. The number of interactions per event is

generally proportional to the data taking rate, which varies between 0.1 and 10 MHz for most runs.

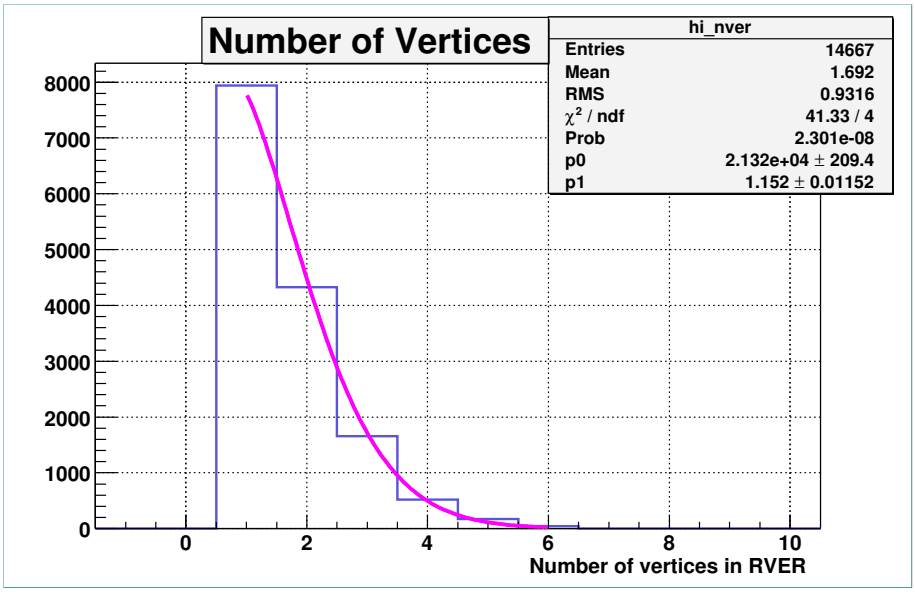

Fig. 30. Example of the distribution of the number of interactions in an event and the Poissonian fit.

We use data from HERA-B runs with two targets in a run, which eliminates the error of $\Delta\alpha$ due to error of knowledge of integrated luminosity and the majority of systematic errors (they cancel out). However, conceptually one can derive the nuclear dependence from one-target runs with different materials, relying on the Monte Carlo simulation of the spectrometer.

Thus the numbers N_{inel}^{X} and N_{inel}^{Y} are obtained by counting the number of primary vertices. The numbers N_{Φ}^{X} and N_{Φ}^{Y} can be obtained in the two following ways:

1) The mass histogram is fitted with a function equal to the sum of a Gaussian for the

signal and a 2nd or 3rd order polynomial for the background. N_{Φ}^{X} is then calculated through the integration of the fitted Gaussian function.

2) Once the fitting is successfully done, the polynomial describing the background becomes available. We calculate the contents of the bins over the background, and add them in the mass range $center\ of\ the\ peak \pm 3\sigma$. Fig. 31 illustrates the procedure. We also note that since we are going to take a ratio later, the exact width of the range ($\pm 3\sigma$) is not critically important - it can be less.

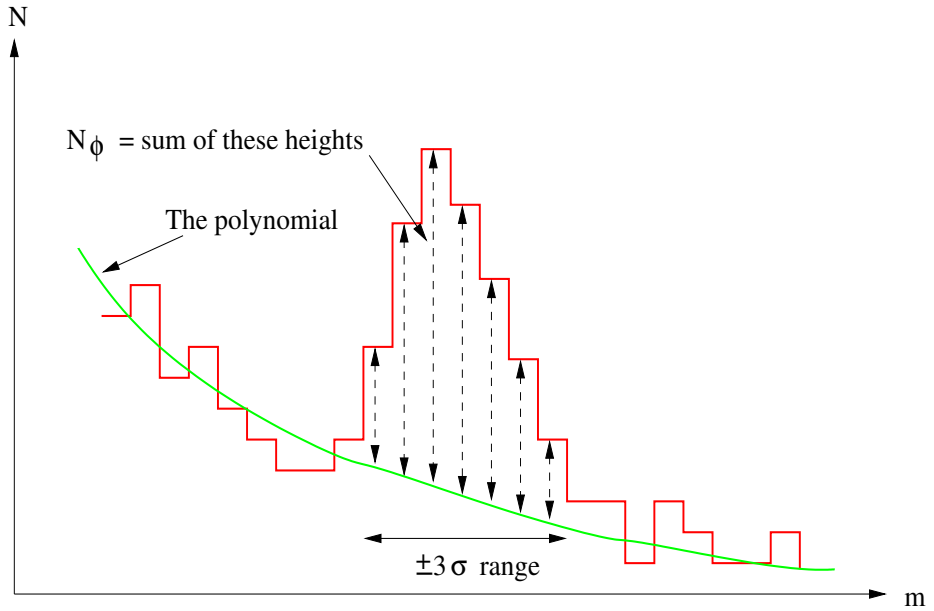

Fig. 31. Obtaining the number of Φ mesons through summation of bin contents.

From the results of fitting of the curves in Fig. 28 and from the analysis program, for C-W material combination we get the following result (see Table 5):

Table 5. Numerical data for the number of Φ-s and number of interactions on different targets.

Histogram in the lower half with ..	***Material***	***A***	***Number of interactions*** N	***Number of Φ mesons*** N_{Φ}	***Φ mass from targets, GeV***	***Φ mass, average***
less entries	C	12.01	$7.73*10^6$	1330	1.01956	1.01957 GeV
more entries	W	183.84	$13.4*10^6$	3060	1.01957	± 80 keV

The efficiencies ϵ_{Φ}^{C} and ϵ_{Φ}^{W} on carbon and tungsten targets were estimated through HERA-B Monte-Carlo [35], and are: 1.455% for carbon and 1.315% for tungsten. The uncertainty of our knowledge of these quantities is unknown, but taking the logarithm of their ratio which is close to 1 in (10) diminishes the effect of this unknown uncertainty on the error of $\Delta\alpha$. The difference in efficiencies can be attributed to the higher multiplicity in case of tungsten, which worsens the reconstruction efficiency of the Φ mesons on the heavier target materials. (A separate study showed that the multiplicity for tungsten target is approximately 1.5 times higher than the multiplicity for carbon target.)

We now have all the required quantities and calculate, according to (10),

$\Delta\alpha = 0.141$.

But this is not yet the final result. The numbers N_{Φ}^{X} and N_{Φ}^{Y} depend on the details of the fitting, which depend on the number of bins of the mass histogram. In

general, other small variations like: taking not the whole data sample but 95% of it; changing the cuts slightly; changing the order of the polynomial used to fit the peaks etc have some effect on $\Delta\alpha$. As an example, Table 6 shows the values of $\Delta\alpha$ through fitting (2nd column), the values of $\Delta\alpha$ through summation of bin contents over the background (3rd column) and the mass of the Φ meson for several binnings of the mass histogram (4th column) for C-W runs . The Particle Data Book [22] lists the mass of the Φ meson as 1.019456 ± 0.00002 GeV and width Γ equal to 4.26 ± 0.05 MeV.

Table 6. Example of dependence of the exponent $\Delta\alpha$ on small variation of parameters (number of bins in this case).

Number of bins of mass histogram	***Exponent, obtained through fitting***	***Exponent, obtained through summation of bin contents***	***Φ's mass, GeV***
95	0.109	0.103	1.01958 ± 0.00008(stat)
96	0.105	0.099	1.01955 ± 0.00008(stat)
105	0.099	0.093	1.01956 ± 0.00008(stat)

Two of the corresponding pictures - for 95 and 96 bins - are shown in the following Figures 32 and 33.

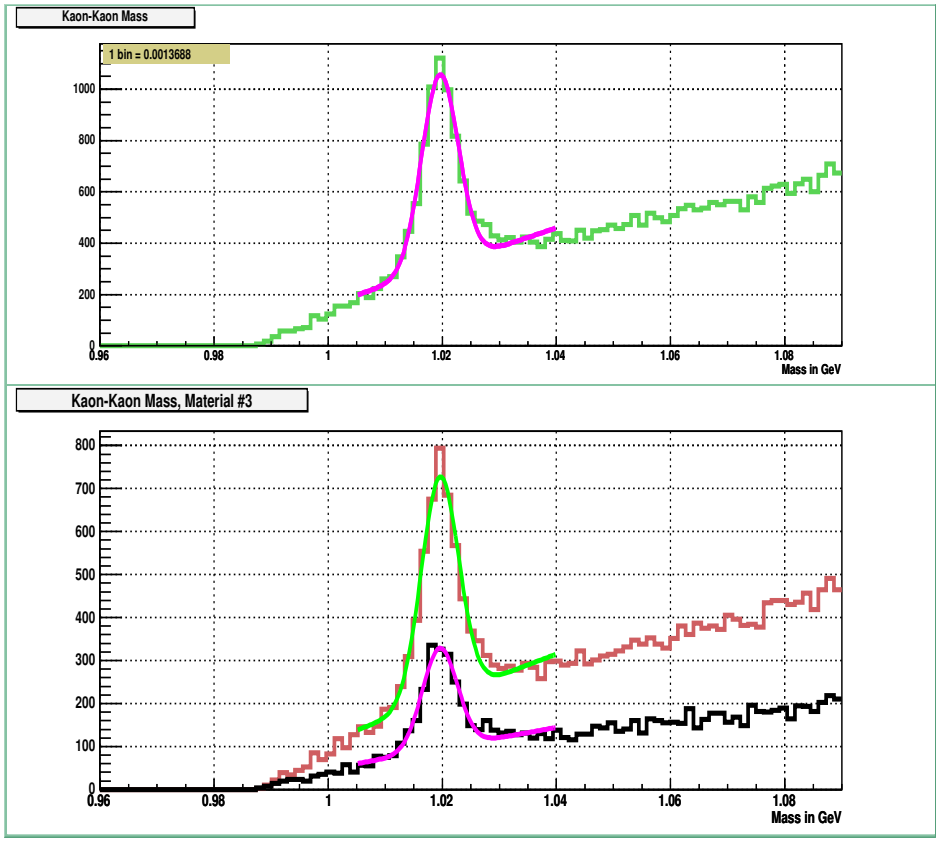

Fig. 32. The Φ peaks on two targets. Number of bins = 95.

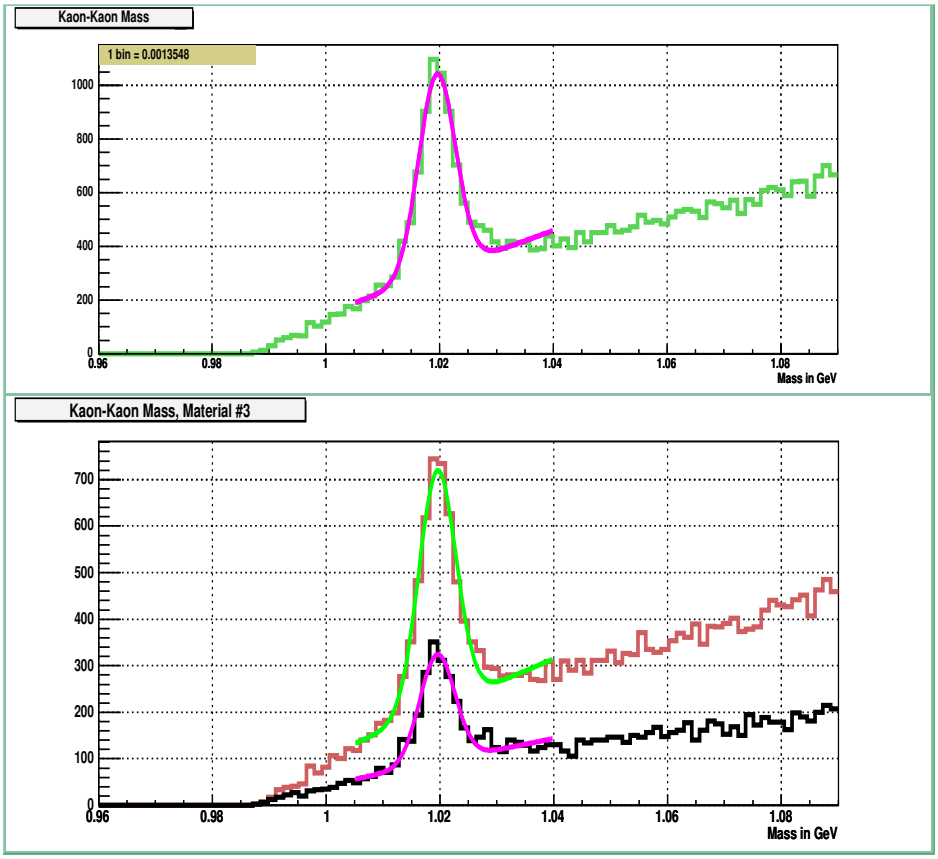

Fig. 33. The Φ peaks on two targets. Number of bins = 96.

Filling out a much larger version of Table 6 for different binnings , we arrive at the following values for $\Delta\alpha_{fit}$ (obtained through fitting), $\Delta\alpha_{bin}$ (obtained through summation of bin contents over the background), m_{Φ} (mass of the Φ meson), and their standard deviations (denoted with δ):

- $\Delta\alpha_{fit}=0.1415;\ \delta(\Delta\alpha_{fit})=0.003$
- $\Delta\alpha_{bin}=0.1396;\ \delta(\Delta\alpha_{bin})=0.003$
- $m_{\Phi}=1.01957\,GeV;\ \delta(m_{\Phi})=80\,keV$

Arbitrarily, we take the arithmetic average of the results of the fitting and bin

counting methods, and get: $\Delta\alpha = 0.141$.

The statistical error of $\Delta\alpha$ can be estimated as follows. In the formula (10), the error in the denominator $\ln\left(\frac{A^Y}{A^X}\right)$ is negligible. Thus the error comes from the ratios $Q = \frac{\frac{N_{\Phi}^Y}{N^Y}}{\frac{N_{\Phi}^X}{N^X}}$ and $\epsilon_{\Phi}^X / \epsilon_{\Phi}^Y$. The statistical error in the ratio of efficiencies is negligible [35].

Let us denote the standard error of Q by $\delta(Q)$ and the relative standard error of Q by $\sigma(Q) \equiv \delta(q)/Q$. $\sigma(Q)$ is determined by the relative standard errors of N_{Φ}^X, N^X, N_{Φ}^Y, N^Y and equals to the sum in quadrature of the standard errors of those numbers, since the four numbers are not correlated: $\sigma(Q) = \sqrt{[\sigma(N_{\Phi}^Y)]^2 + [\sigma(N^Y)]^2 + [\sigma(N_{\Phi}^X)]^2 + [\sigma(N^X)]^2}$. Assuming that each of the numbers N has a relative standard error equal to $1/\sqrt{(N)}$ and using the data from Table 6 , we calculate $\sigma(Q) = 0.033$. We also calculate Q to be 0.747. To propagate the error $\delta(Q) = Q\sigma(Q) = 0.025$ through formula (4) for $\Delta\alpha$, we take the differential:

$$\delta(\Delta\alpha) = \left| \frac{\partial}{\partial Q} \left(\frac{\ln(Q) + \ln\left(\epsilon_{\Phi}^W / \epsilon_{\Phi}^C\right)}{\ln(A^Y / A^X)} \right) \right| \delta(Q) = \frac{\sigma(Q)}{\left|\ln(A^Y / A^X)\right|} = \frac{0.033}{2.73} = 0.012$$

Thus, for carbon-tungsten combination we have:

$$\Delta\alpha = 0.141 \pm 0.012(stat)$$

We proceed now to the estimation of the systematic error $\delta_{sys}(\Delta\alpha)$ of the quantity $\Delta\alpha$. As mentioned above, the main sources of the error cancel out in the formula (10) for $\Delta\alpha$. There is, of course, an error associated with $\epsilon_{\Phi}^{X}/\epsilon_{\Phi}^{Y}$, but currently we are unable to estimate it. We assume that error to be zero.

To estimate the remaining systematic errors, we look at carbon-carbon runs, i.e. at runs with two active wires, each of which is made of carbon. HERA-B has taken a substantial sample of runs with two target wires each made of carbon. Should there be no systematic error, the two ratios - $N_{\Phi}{}^{1}/N_{inel}^{1}$ and $N_{\Phi}{}^{2}/N_{inel}^{2}$ - would be equal within statistical fluctuations. Here superscripts 1 and 2 denote the target numbers, not the target materials (target material is the same). It is impossible to extract A-dependence from C-C runs only, but the evaluation of the ratio of these two ratios, the quantity already denoted by Q, gives us a good estimate of the remaining systematic error of $\Delta\alpha$. In case of no errors, $Q=1$.

To accomplish the error estimate, we obtained the number of Φ mesons on each of the carbon wires in exactly the same way we have obtained them for C-W runs. Exactly the same way means: use the same programs, apply the same cuts, fit the histograms with the same function. The corresponding curves are shown in Fig. 34.

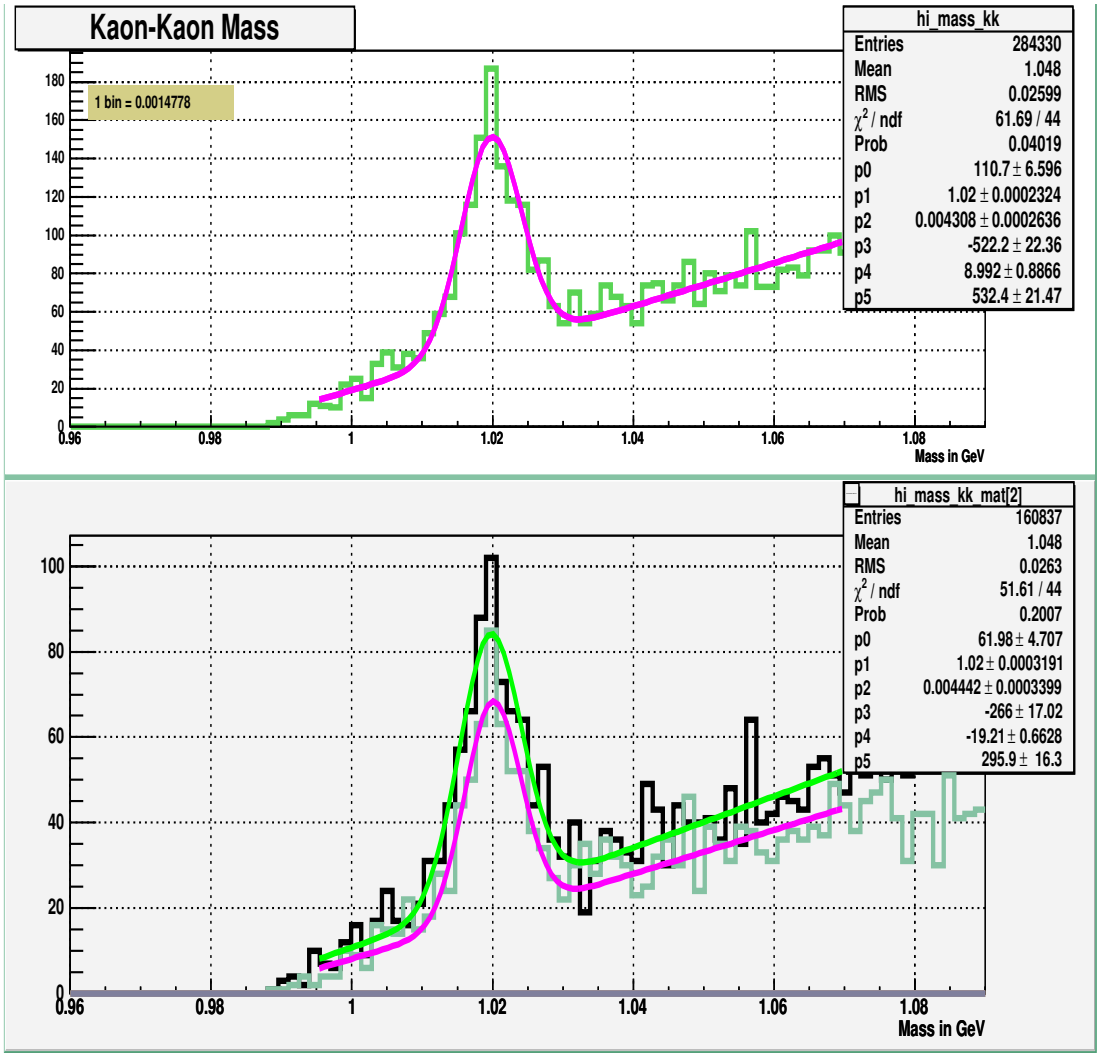

Fig. 34. Φ peaks obtained in C-C runs.

The number of events for these runs is less than that for C-W runs, which explains the higher fluctuations of the bin contents of the histograms. As an example, Table 7 shows the ratio Q for three binnings, obtained, like in Table 6, through two methods: fitting and summation of bin contents.

Table 7. The ratio Q , obtained in C-C runs from 11 million events (the whole available sample).

Number of bins of mass histogram	***Q, obtained through fitting***	***Q, obtained through summation of bin contents***
73	1.082	1.046
74	1.057	1.039
75	1.002	0.992

Because of the smaller number of entries in C-C histograms compared to that in C-W histograms, the histograms are less smooth, and the method of summation of bin contents provides smaller deviations of Q . Filling out a larger version of Table 7 and using the third column, we come to a conclusion that Q differs from 1 typically by 3% to 5%, having an average value 1.04. Thus, we now have estimated the error of Q for determination of error of $\Delta\alpha$: $\sigma(Q)$ is around 4%. The deviation from 1 comes from a combination of systematic and statistical grounds, but we cannot separate them.

As earlier, we have also estimated the statistical uncertainty of Q in these C-C runs using the second method - by adding component errors (quantities $1/\sqrt{N}$) in quadrature. We get $\sigma(Q)\approx 8\%$.

Again, we take the arithmetic average of these estimates and declare, that the relative error in our knowledge of Q in C-C runs is around $\sigma(Q)\approx 0.06$.

This number determines our systematic error when we estimate the error of $\Delta\alpha$ for C-W runs. Propagating now this error $\delta(Q)=Q\sigma(Q)$ through formula (10) for $\Delta\alpha$, we obtain for C-W runs an estimate for systematic error:

$$\delta_{sys}(\Delta\alpha)=\left|\frac{\partial}{\partial Q}\left(\frac{\ln(Q)+\ln\left(\epsilon_{\Phi}^{X}/\epsilon_{\Phi}^{Y}\right)}{\ln(A^{Y}/A^{X})}\right)\right|\delta(Q)=\frac{\sigma(Q)}{\left|\ln(A^{Y}/A^{X})\right|}=\frac{0.06}{2.73}=0.022$$

Of course there are other sources of systematic errors. We could not reliably estimate them. One candidate was, however, investigated: the dependence of the parameter $\Delta\alpha$ on the trigger type. That is, we looked whether $\Delta\alpha$ varies when the trigger type used in runs changes, other things kept unchanged as much as possible. There were several trigger types used. It appears that besides one trigger type (called "interaction"), there is no significant variation in the magnitude of $\Delta\alpha$. Anyhow, the interaction-triggered runs with two targets are not much in quantity and they, combined, do not yield significant Φ peaks. They were excluded from this study.

Thus, finally, for C-W combination in this study we have obtained:

$\Delta\alpha=0.141\pm0.012(stat)\pm0.022(sys)$.

Besides runs with carbon and tungsten, there were two-target runs with titanium, palladium and alloy of tungsten and rhenium. Runs with palladium have very small number of events and the Φ meson peak could not be observed. The peak could be reconstructed for C-Ti runs. The following figure (Fig. 35) shows the peak.

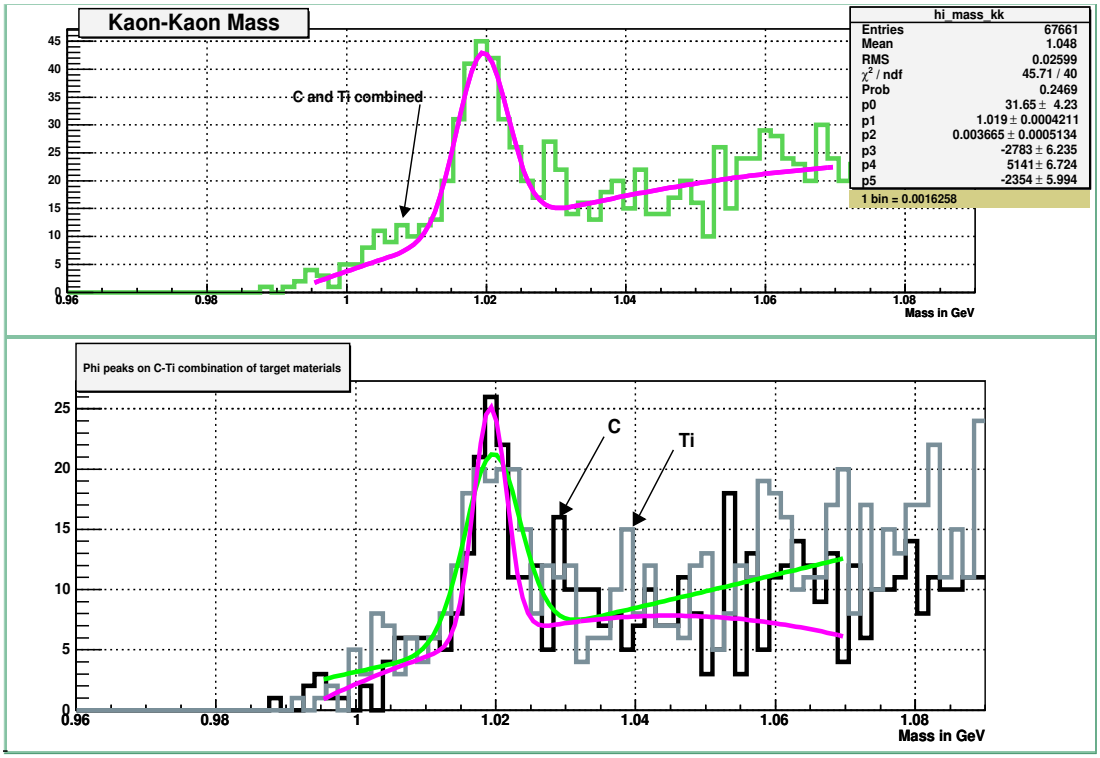

Fig. 35. Φ peaks obtained in C-Ti runs.

The numbers of Φ mesons under the peaks are substantially smaller than those under the peaks for C-W combinations, which is explained by the smaller number of events (around 2.4 million). Under each peak there are around 80 background-subtracted entries.

We do not know the Monte-Carlo estimate for ϵ_{Φ}^{Ti}. We can assume it to be equal to the arithmetic mean of the values of carbon and tungsten. Applying the same techniques that were described above for C-W runs for finding statistical error $\delta(\Delta\alpha)$, we find the statistical error to be $\delta(\Delta\alpha)\approx 0.1$. Systematic error is, naturally, the same. Thus, for C-Ti runs we have obtained:

$$\Delta\alpha = 0.155 \pm 0.1(stat) \pm 0.022(sys)$$

We see that the statistical error is comparable to the magnitude of $\Delta\alpha$, and is much greater than the error in C-W runs. For this reason, the result for $\Delta\alpha$ from C-Ti runs has much less "weight" than that for C-W runs. But we still keep it since there are no measurements in the literature for carbon-titanium combination.

We have also attempted to obtain the A-dependence from a set of runs with the first target made out of carbon and the second target made out of an alloy of 90% tungsten and 10% of rhenium. The atomic numbers of W and Re are very close: 183.8 and 185.2, respectively. We assume that the efficiency of Φ meson reconstruction for the alloy and for tungsten are the same: $\epsilon_{\Phi}^{W+Re} = 1.315\%$. The alloy has $A = 184.5$. Fig. 36 shows the Φ peaks.

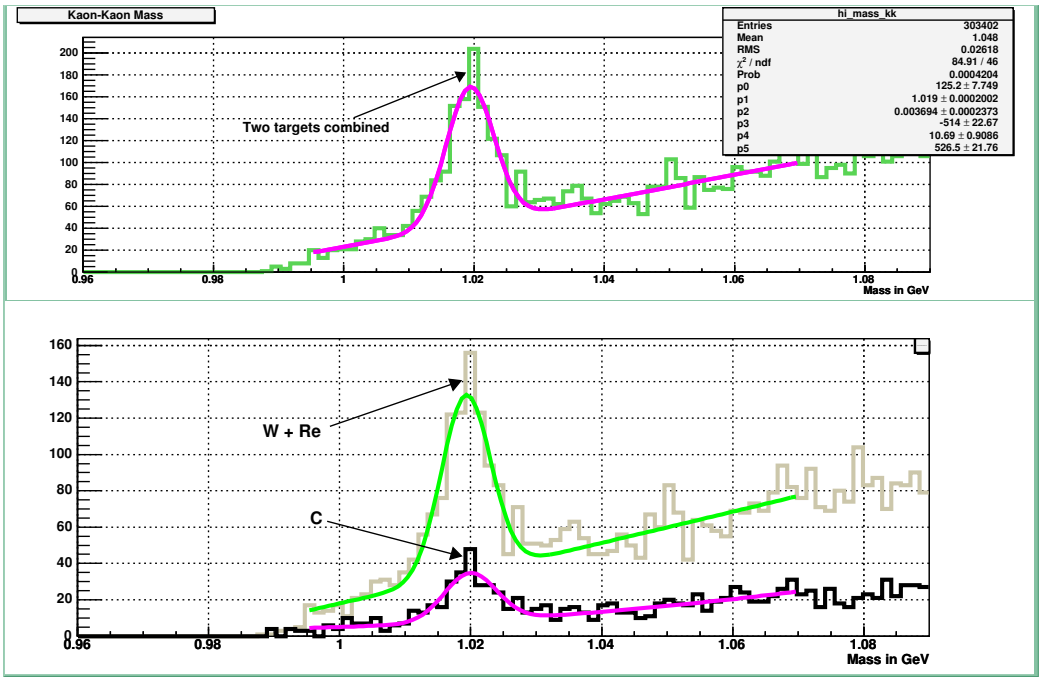

Fig. 36. Φ peaks obtained in C - (W+Re) runs.

We obtain $\Delta\alpha$ and its errors in the same way we have done for C-W and C-Ti combinations. We get:

$$\Delta\alpha = 0.187 \pm 0.08(stat) \pm 0.022(sys)$$

This number is somewhat higher than the value of $\Delta\alpha$ for C-W combination. One possible explanation is that the ratio of activities of targets, expressed in terms of ratio of the numbers of interactions on each of the targets, is substantially different from that of the two previous material combinations. This may affect the efficiency of the reconstruction software, yielding different number of reconstructed tracks - both general tracks and K meson tracks that yield the Φ meson - depending on the activity ratio. We cannot estimate the magnitude of this effect here.

Another explanation of the different value of $\Delta\alpha$ is that the A-dependence, described through a simple power law, is too crude, and, for example, the geometrical form of the nucleus plays some role. One has to investigate a set of different materials and alloys to get the answer for that.

One more explanation is that that the tungsten nuclei in alloy and the tungsten nuclei in tungsten bulk behave differently in p-A interaction, e.g., because of different spin orientation of the nuclei which depends on the crystalline structure of the material.

4.4. Comparison with other experiments

Here we will discuss two experimentally obtained dependences: proton-nucleus (or

neutron-nucleus) cross-section and the A-dependence of specific hadrons production. Both are important for verification, comparison and usage of our results.

In this work we have studied the A-dependence of Φ meson production per inelastic interaction, i.e., looked at: "Once an inelastic interaction occurs, is there an A-dependence of the Φ meson production, or do all nuclei behave the same way?" Looking at A-dependence in this way, as we have told, eliminates the majority of the systematic errors.

All the experimental papers we could find study just the A-dependence. In their cases, power law dependence is the model. This allows comparison of our and their results by a simple subtraction: $\Delta\alpha = \alpha_{hadron} - \alpha_{inel}$. Later in this section we will demonstrate that experimentally obtained results can be summarized as $\alpha_{inel} \approx 0.72$. When comparing the exponents obtained, we must keep in mind that the experiments are different, the main differences being in the beam energy and the x_F range considered.

Proton-nucleus cross-sections. As it is anticipated from simple geometrical considerations, when the free path of the projectile in nuclear matter is roughly equal to the nucleon size, a power law dependence with exponent close to 2/3 is anticipated; see 1.5 above and [12]. A number of experiments have been carried out to verify the power law and determine the exponent. The experiments themselves are straightforward, though the determination of errors is not. In most cases, thin foils of several materials having absorption length around 20% of the total radiation length are used as targets, either simultaneously (like in HERA-B), or sequentially.

The authors of [37] studied neutron projectiles and Be, C, Al, Cd , Pd and other targets at projectile momenta 30-300 GeV. Their results can be summarized as $A^{0.77\pm0.01}$ dependence of the total inelastic cross-section for momenta above 30 GeV.

The authors of [38] studied the cross-sections of pion, kaon and proton absorption in Li, C, Al, Cu, Sn and Pb at 60-280 GeV. The absorption cross-section is not exactly equal to the inelastic cross-section we use in this work; they are; however closely related, and, extrapolated to our energies (920 GeV), are close to each other. They again parametrize the nuclear dependence as $\sigma(A)=\sigma_0 A^{\alpha}$ and have obtained the exponent to be from 0.71 to 0.79 depending mostly on projectile's energy, with typical error ±0.02.

In [14], considering the same cross-section at HERA-B energies (actually, at the energy 820, not 920 GeV, since it was the energy of the proton beam when HERA-B has started), the authors, based on the material accumulated, find that 0.7 value for α_{inel} is probably not the best and that the value should be higher.

The author of [39] did a compilation of the existing results and extrapolated them to the HERA energy. His result for A-dependence of the total inelastic cross-section is that the exponent is $\alpha_{inel}=0.7111\pm0.0011$ for p-A collision. The exponent for total cross-section is also obtained: $\alpha_{total}=0.7694\pm0.0012$.

We hence may finally conclude that the best estimate for the total inelastic cross-section in our case is $\sigma\propto A^{0.72}$. (It was shown experimentally that the exponent depends weakly on the hadron type, the energy range and the x_F range [12, 14, 36-38, 40], varying in most cases by ±0.1.)

Specific hadrons production cross-sections. In [40], the A-dependence of Φ meson production was studied in 120 GeV antiproton beam for Be and Ta. The authors used multiple thin foils made of those materials, which allowed them to assign the mesons to the materials where they were produced. They obtained $\alpha_{\Phi} = 0.86 \pm 0.02$. Assuming 0.72 exponent for inelastic cross-section's A-dependence, this result is translated into ours as $\Delta\alpha = 0.14$. They have also obtained the A-dependence in π^+ beam, which appeared to be close to the value in antiproton beam.

The authors of [13] studied the production of Ξ^- and $\overline{\Xi^+}$ in 250 GeV π^- beam for Be, Al, Cu, and W. They used several thin foils as targets. The obtained dependence is $\alpha = 0.924 \pm 0.02(stat) \pm 0.025(sys)$. Also, in their article they discuss and agree with the power law parametrization, and use it for A-dependence. This result is translated into our per interaction frame as $\Delta\alpha = 0.2$. But, of course, there is no strong ground for comparison, since they studied another particle.

In [41], the D^0 production in 800 GeV/c proton beam was studied using thin strip targets of Be and Au. The result is $\alpha = 1.02 \pm 0.03 \pm 0.02$, or, in our per interaction frame, $\Delta\alpha = 0.3$. Again, this result, besides the technique used to obtain the A-dependence, is not directly comparable to ours.

The authors of [11] have studied the mass of the Φ meson. Investigating the mass of the meson produced in two materials, the authors came to the conclusion that it does not differ from the mass of "free" Φ meson as produced in electron colliders and equals to 1.01924 GeV ± 280 keV. Here are our results, for comparison: same mass of mesons

produced in C and W, equal to 1019.57 MeV ± 80 keV(stat). (The Particle Data Book [22] lists the mass as 1.019456 MeV ± 20 keV.)

The general conclusion that we arrive at is the following: the A-dependence of the cross-section of the Φ meson production we have obtained agrees with and expands the range of similar dependences obtained in other experiments.

Chapter 5. A simple Monte Carlo study of the Φ meson production in a proton-nucleus collision

5.1. The known parameters describing the proton, nuclei and their interactions at high energies

As we have described above, the mechanisms of s, $\bar{s}$ and Φ production are complex and difficult to investigate directly. However, much is known about hadron-hadron interactions in general, which allows us to develop a simplified Monte Carlo simulation of the processes we investigate and to arrive at A-dependence of the Φ yield through that simulation [5, 42]. In the following paragraphs we summarize the necessary knowledge.

The inelastic cross-section of p-p interaction at energies around 920 GeV is 30-40 mbarn [1].

The radius of a proton or a neutron r is approximately equal to 0.8 fm [43, 44].

The naive nucleus model, which is a model in which nucleons are placed compactly in the nucleus with almost no gaps between them, is close enough to reality and is often used, at least for A-dependence studies with several hundred GeV hadron projectiles [45].

The radii of nuclei, in general, follow the rule: $R(A) \approx rA^{1/3}$. For example, for

^{40}Ar, the nuclear radius is 3.3 fm, which corresponds to the distance between the centers of the nucleons around 1.55 fm. Same quantities for ^{205}Pb are 5.7 fm and 1.54 fm, and for ^{238}U they are 7.2 fm and 1.86 fm [46, 47].

The production cross-section of Φ in p-p collision equals 1 mbarn at 920 GeV [8].

The lifetime τ of the Φ meson is around $1.5*10^{-22}$ s. In the HERA-B, the typical value of γ of the produced Φ mesons is around 20. The average flight length then is equal to $c\tau\gamma \approx 1000\, fm$, which is much greater than the sizes of nuclei. This means that inside the nucleus a spontaneous decay of the Φ meson almost never occurs.

In reality, the propagation mechanism of produced Φ mesons in nucleus is complex and is a topic of several theoretical investigations (see 1.5). Here, for the purpose of our Monte Carlo study, we assume that the produced meson can follow only one of the two paths: be absorbed (annihilated) in collisions with nucleons on its path, or exit the nucleus and be detected.

For our Monte Carlo simulation, we would like to transform all quantities to a discrete "per nucleon" basis. From the numbers brought above, one can deduce that the absorption length of a proton projectile in nuclear media is $\lambda = (n\sigma)^{-1} \approx 1\, fm$, where n is the concentration of nucleons. We use the quantity λ to find out that, per nucleon, the absorption probability of the projectile (i.e., the probability of an inelastic interaction) is approximately equal to 0.8. Similarly, the probability of Φ meson production in a p-p inelastic interaction can be estimated as 0.04.

With these estimates in hand, we put forward and develop the following simple Monte Carlo model for obtaining the A-dependence of Φ meson production.

5.2. The constructed nucleus and the basic geometry

A nucleus consists of A nucleons, compactly packed. We introduce a coordinate system as follows. The first nucleon is at (0, 0, 0); the flux of projectiles starts at $z=-\infty$ and propagates parallel to the z axis in positive direction. There is a particle detector at $z>R$ which detects all produced Φ mesons and all survived projectiles at $z>R$, where R is the nuclear radius. We do not trace other particles (the X in $projectile+nucleon\rightarrow\Phi+X$). All moving particles move parallel to the z axis. We also assume zero transversal size of the projectiles, for simplicity only.

We build the nucleus by placing nucleons one by one in a way that after each placement the radius of the newly formed nucleus is minimum possible. In addition, we require a small gap, equal to 5% of r, between any nucleons in the nucleus. Fig. 37 shows the objects in Monte Carlo simulation. Fig. 38 shows a three-dimensional view of a sample nucleus with A=80. In Fig. 38, the centers of the spheres represent the centers of the nucleons, but the radius of the spheres is made smaller than the radius of the nucleon to make the picture better visible.

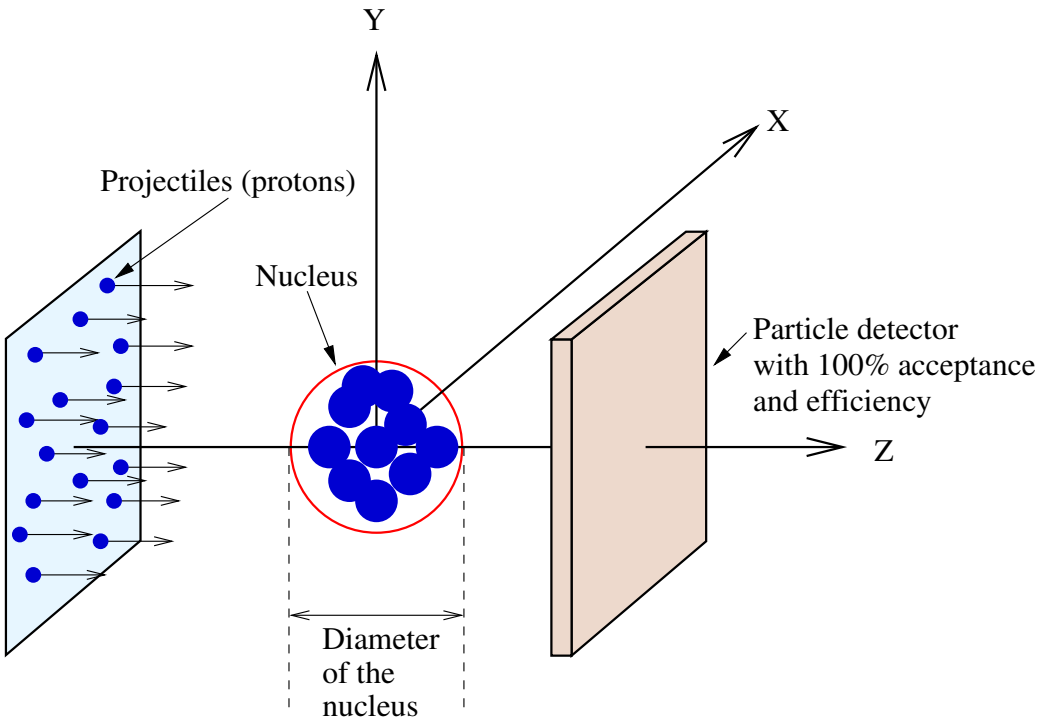

Fig. 37. Spatial relations in Monte Carlo simulation.

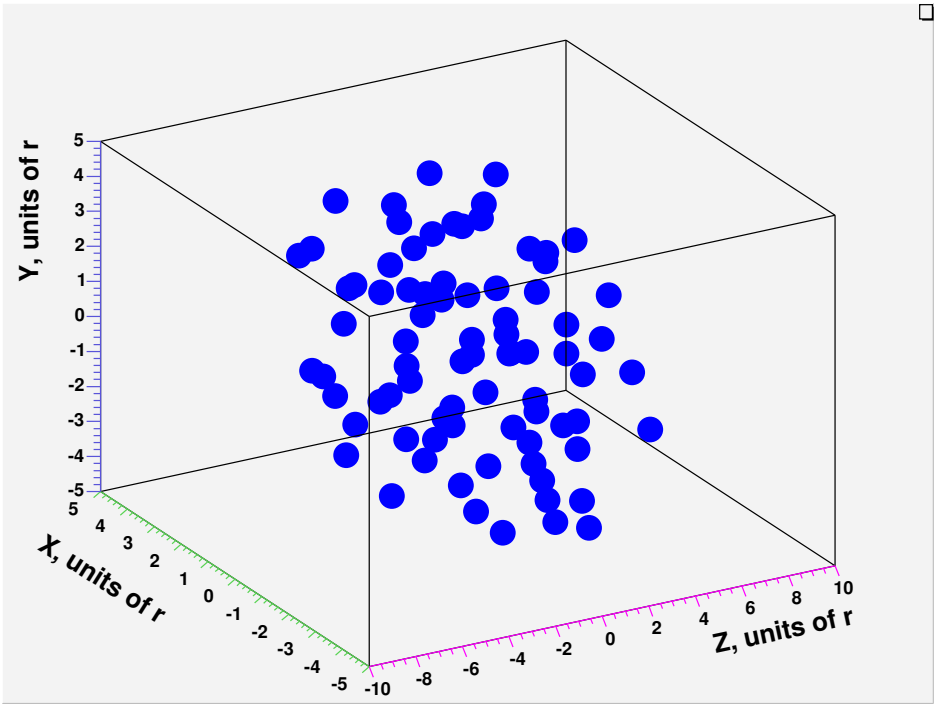

Fig. 38. A simulated nucleus with A=80.

The simulation of the interaction is done according to the following simple logic. Once a projectile hits a nucleon of the nucleus, there are only two possible outcomes: the interaction is inelastic with probability $P_{inel} \approx 0.8$, or there is no interaction and the projectile hits the next nucleon on its way (if there is one). In the case of an inelastic interaction, the projectile (but not the nucleon) annihilates, and a Φ meson is produced with probability $P_{phi\_gen} \approx 0.04$. The Φ mesons are believed to be produced through gluon fusion mechanism (see 1.4), but the probability of Φ meson production 0.04, which we use here, is obtained through the experimentally measured production cross-section around 1 mbarn [8].

The Φ meson begins traversing the remaining nucleons on its way. At every nucleon, it has a chance to be absorbed with probability $0 \leq P_{phi\_absorb} \ll 1$.

Many thousands of projectiles are generated on a two-dimensional grid on the left-hand side of the nucleus. Each of them is traced to the right in the way described above. The total size of the grid is larger than the size of the largest nucleus under consideration. The Φ mesons that finally emerge are counted. Also, the total number of survived projectiles in the beam after the nucleus is counted. Fig. 39 shows the particle distributions in planes parallel to (x, y) plane. The upper left picture shows the generated Φ mesons and the projectiles. The upper right picture shows only the Φ mesons as they arrive onto the detector. The lower picture shows the shadow of the projectiles on the detector.

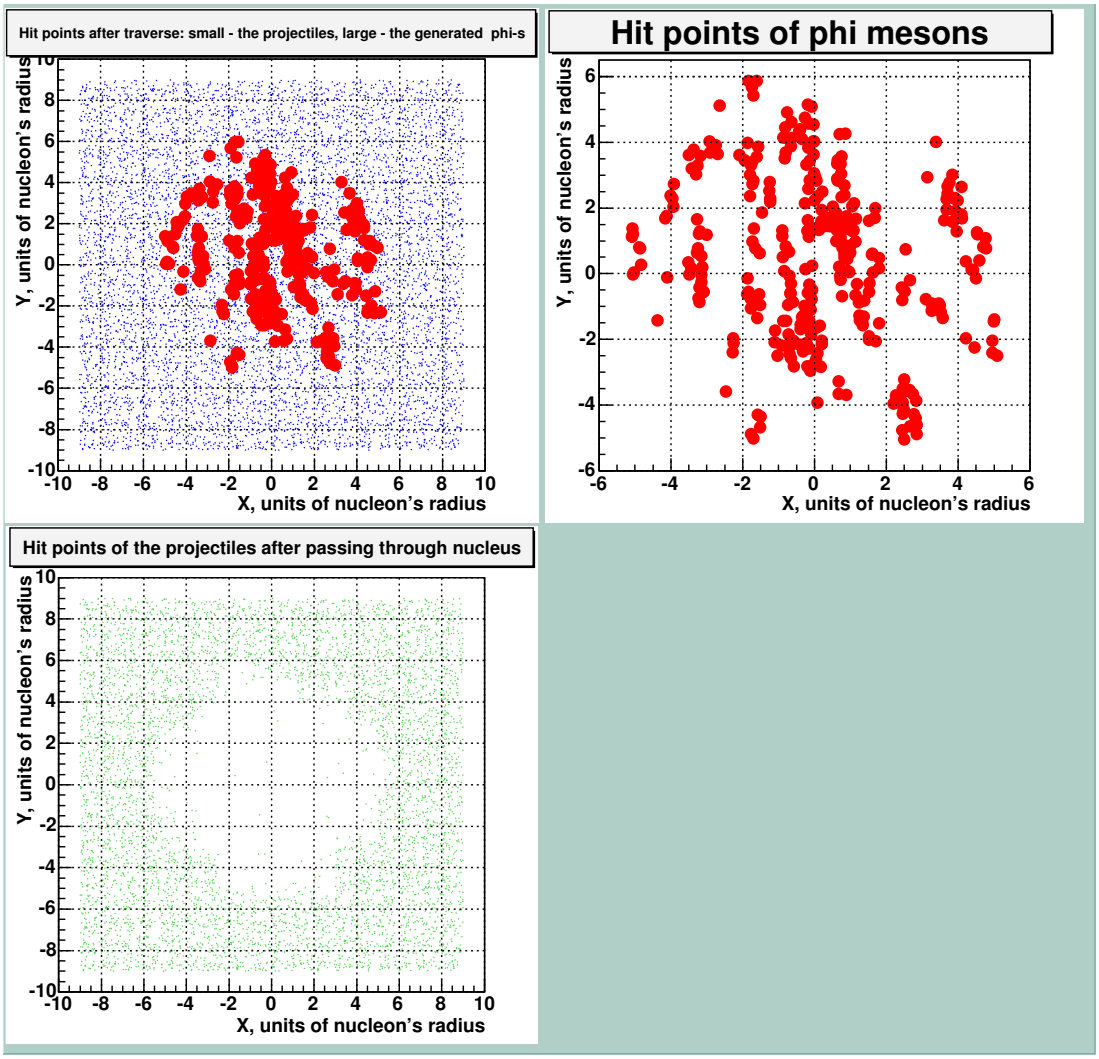

Fig. 39. Sample particle distributions in planes perpendicular to the z axis.

5.3. Obtaining the simulated A-dependence

We obtain the the A-dependence in this model by plotting the number of detected Φ mesons versus A and fitting the curve.

Before we proceed to the final result, we would like to show the successful

reproduction of two well-known extreme-case results [13]. We show these results only for proof and for estimation of the expected accuracy of $\Delta\alpha$ within this model.

One extreme case is when $P_{inel}=1$ and there is no absorption of the produced mesons. The projectile is absorbed at the surface of the nucleus, on the left hemisphere. The area of this surface is proportional to $A^{2/3}$, and so is the number of inelastic interactions. Therefore, the number of generated Φ mesons N_{Φ} is also proportional to $A^{2/3}$.

The other extreme case is when $0<P_{inel}\ll 1$ and again there is no absorption of the produced mesons, i.e., we have the case when the absorption length of the projectiles is much larger that the size of the nucleus. Here, the number of absorbed projectiles and N_{Φ} are proportional to the volume of the nucleus which is proportional to A .

Figures 40 and 41, obtained through simulation, demonstrate these dependences. In Fig. 40, we have set $P_{inel}=1$. In Fig. 41, we have set $P_{inel}=0.08$. (Note that we cannot set the last probability to zero, because we will get a trivial zero result.) In both cases, we have set the probability of the generation of a Φ meson in an inelastic interaction to 0.04, and have set no absorption of the Φ mesons. The obtained exponents - 0.69 and 0.97 - are close to the expected values 0.67 and 1.

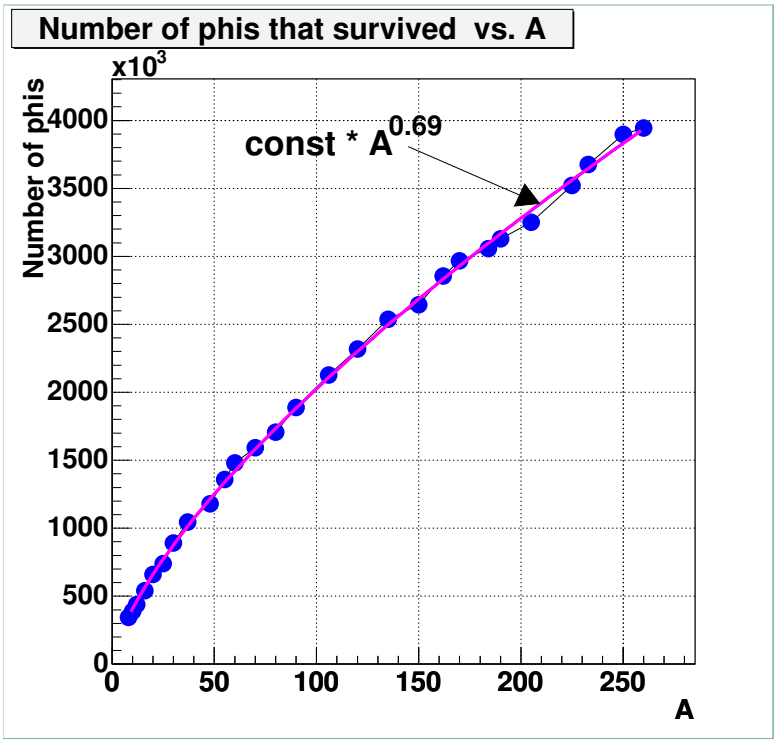

Fig. 40. A-dependence of Φ production in case of 100% projectile interaction probability.

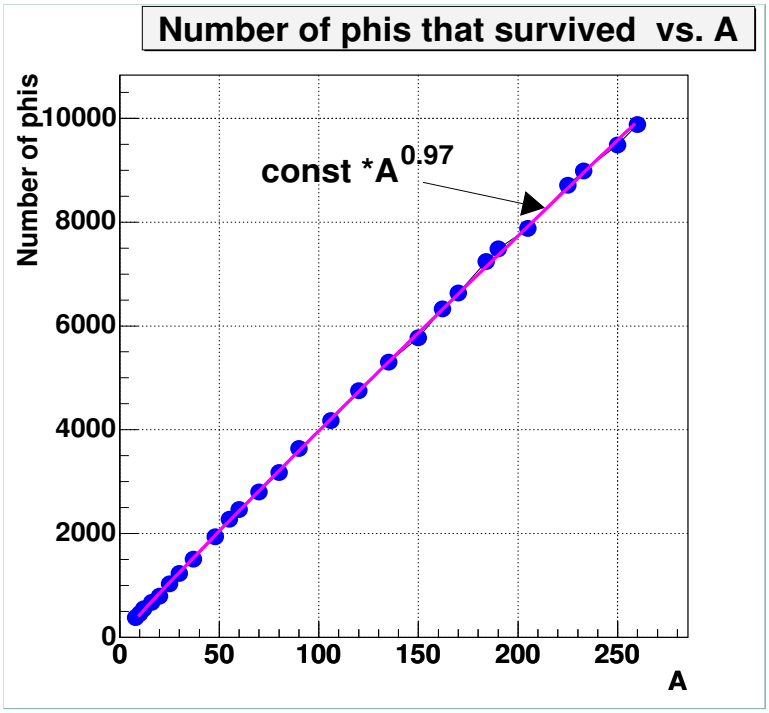

Fig. 41. A-dependence of Φ production in case of 8% projectile interaction probability.

Below is the demonstration of the main point of our Monte Carlo simulation: it is possible to closely reproduce the experimental results on the A-dependence within a simple model simulation. We will do it schematically, with values close but not exactly equal to the experimentally obtained ones.

Our experimental (not Monte Carlo) results can be formulated, in a brief form, as follows: the cross-section of Φ meson production in a proton-nucleus inelastic collision is proportional to $A^{\Delta\alpha}$, where the exponent $\Delta\alpha$ varies between 0.14 and 0.19. Assuming, after 4.4, that the cross-section of proton-nucleus inelastic collision itself is proportional to $A^{\approx 0.72}$, we conclude, that, in a proton beam, the cross-section of Φ meson production is proportional to $A^{\approx 0.85}$. The Monte Carlo model we have developed has three empiric parameters:

1) Probability of p-nucleon inelastic interaction $P_{inel} \approx 0.8$.
2) Probability of generation of a Φ meson in such an inelastic interaction $P_{phi\_gen} \approx 0.04$.
3) Probability of absorption of the produced Φ meson by a nucleon $P_{phi\_absorb} \approx 0$.

Numerical values of the parameters that we use in Monte Carlo simulation are obtained from a series of high energy physics experiments, or are our best estimates. Using these values in simulation (Monte Carlo run), we obtain the dependence as $A^{0.71}$, as the Fig. 42 below shows.

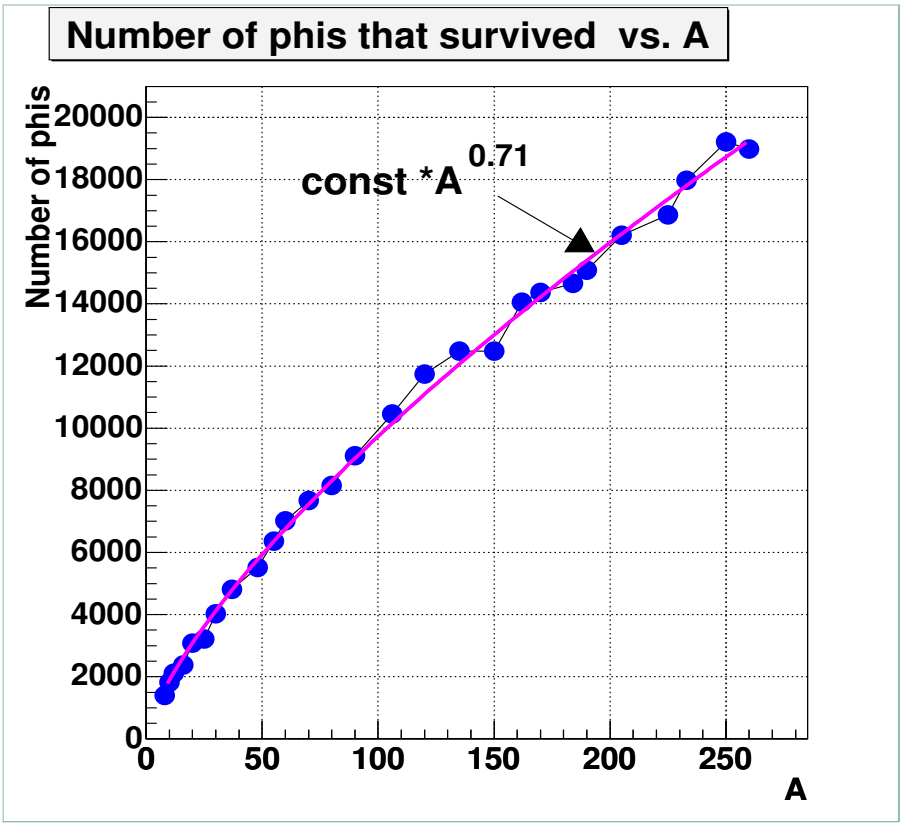

Fig. 42. A-dependence (number of produced Φ mesons) with experimental values of parameters.

The dependence $A^{0.71}$ is off from what we have obtained earlier by analyzing the HERA-B data: namely, the exponent is close to 0.86 for the most representative C-W data sample. By varying the magnitudes of the three parameters, it is possible to achieve $A^{\approx 0.86}$ dependence of Φ meson production within the frame of the simple model we use. We explored two possibilities.

The first possibility is setting the third parameter - probability of absorption of the Φ meson - to a negative value equal to -0.2. Negative absorption, as usual, denotes amplification. We interpret it as production of Φ mesons not only in initial proton-nucleon collision, but also later by the other products of the initial collision when they

propagate through the nucleus, or in the quark-gluon plasma formed. The obtained curve with the value of the exponent of the fitted function equal to 0.85 is shown in Fig. 43.

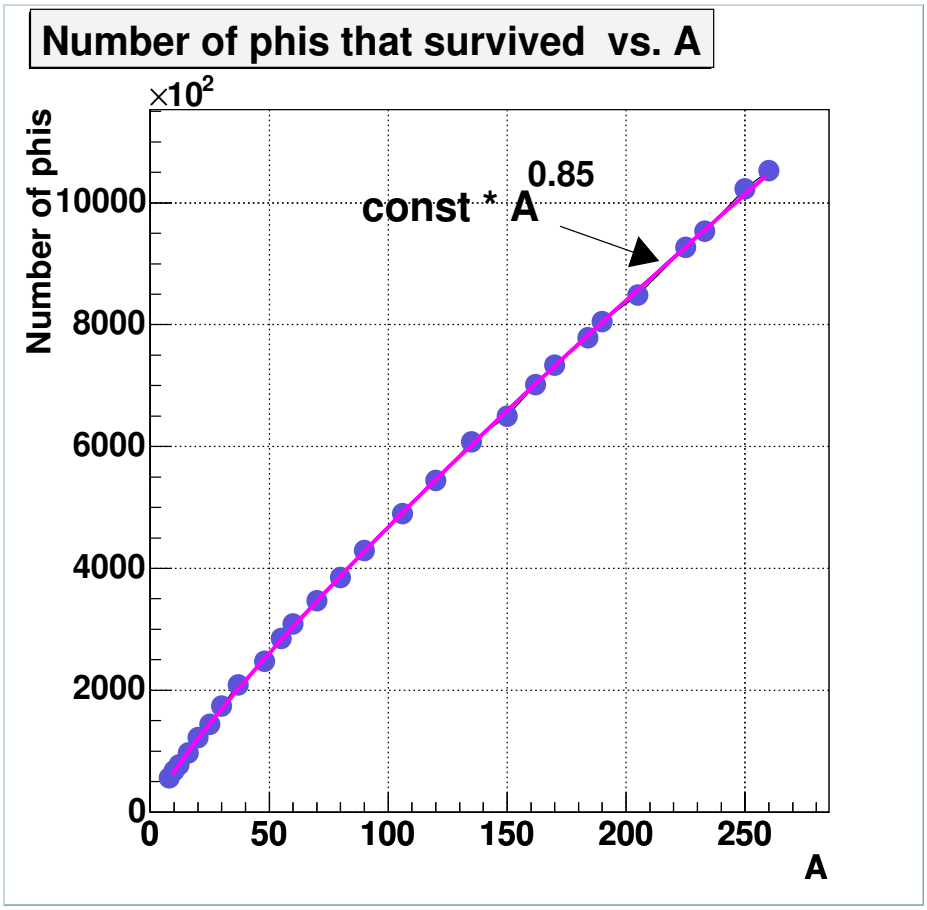

Fig. 43. Setting $P_{phi\_absorb} = -0.20$

The second possibility is setting the first parameter - probability of inelastic p-p collision - to 0.3 instead of 0.8.

We summarize the Monte Carlo results as follows. The simple model we have used

already provides a reasonable value for the power law's exponent, and by tuning parameters it is possible to achieve the same exponent as from HERA-B data. The model does not answer, naturally, which values of parameters are more realistic, but it imposes constraint over the parameters (we did not investigate the constraint in more detail other than obtaining two points of it).

Chapter 6. Conclusions

We have developed a method to study the A-dependence of the Φ meson production in an inelastic event in proton-nucleus collisions at 920 GeV. The method excludes most errors associated with Monte Carlo simulation and does not require knowledge of the integrated luminosity.

As common in nuclear physics, we have parametrized the dependence as $\sigma = \sigma_0 A^{\Delta\alpha}$ and obtained the following values of $\Delta\alpha$ for several material combinations:

Table 8. Summary of results for A-dependence.

Material combination	$\Delta\alpha$ ***(per inelastic interaction)***
C - W	$\Delta\alpha = 0.141 \pm 0.012(stat) \pm 0.022(sys)$
C - Ti	$\Delta\alpha = 0.155 \pm 0.1(stat) \pm 0.022(sys)$
C - (W+Re alloy)	$\Delta\alpha = 0.187 \pm 0.08(stat) \pm 0.022(sys)$

Fig. 44 shows the obtained $\Delta\alpha$ for the three cases, as a function of A:

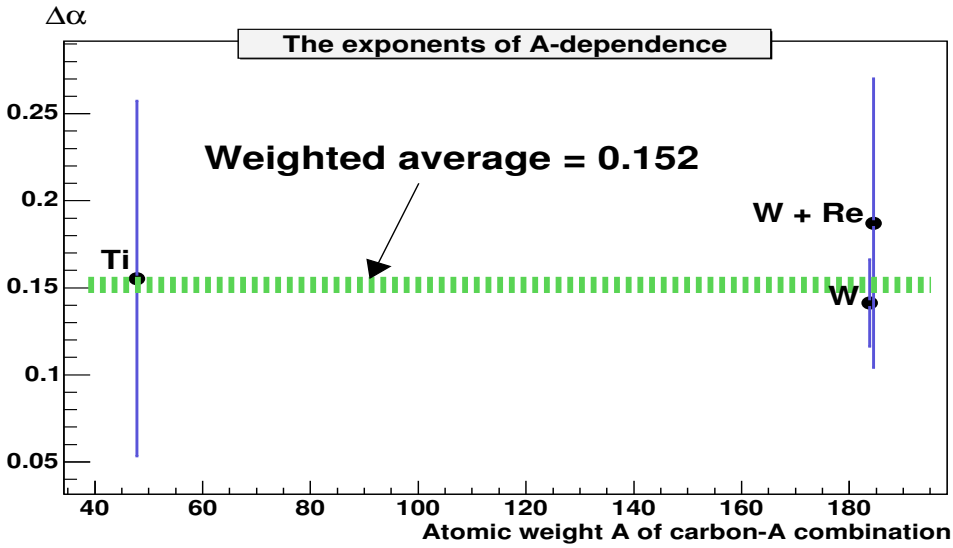

Fig. 44. The obtained exponents $\Delta\alpha$ from all material combinations studied.

As a by-product, the mass of the Φ meson is obtained when it is generated in C and W. The mass of the meson inside the nucleus differs from that in the free space because of strong interaction of the Φ meson and the nuclear medium, and is less inside by an order of 1 MeV [49]. Once the Φ meson decays inside the nucleus, the reconstructed invariant mass of it will be also less compared to the mass in case of a meson decaying outside. An estimate based on the flight length of the Φ mesons at HERA-B and the sizes of the nuclei (see the numbers in 5.1) shows that roughly 0.4% of decays occurs inside. This will result in a shift of the reconstructed mass around 4 keV - a number which is far below the mass resolution in our study. We observed the same mass in C and W within the errors of our measurement to be 1.01957 GeV ±80 keV(stat). (The systematic error has not been studied.)

A simple Monte-Carlo simulation with three parameters: - (1) probability of p-p

inelastic interaction; (2) probability of Φ production in a p-p inelastic collision; (3) probability of absorption of the Φ meson by a nucleon - reproduces the experimental A-dependence and constrains the parameters.

7. References

[1] Donald H. Perkins, *"Introduction to High Energy Physics"*, Addison-Wesley Publishing Company, Inc; third edition, 1987, 449 p.

[2] A. Hosaka, H. Toki, *"Chiral bag model for the nucleon"*, Phys. Rept., v. 277, (1996), pp. 65-188.

[3] J. Ivarsson, *"Potential for B-physics measurements with a fixed-target proton-collision experiment"*, Doctoral thesis, Lund University, ISBN 91-628-3661-7, LUNFD6/(NFFL-7173), (1999).

[4] P. Shukla, "*Glauber model for heavy ion collisions from low energies to high energies"*, arXiv:nucl-th/0112039 v1 13 Dec 2001.

[5] Marco van Leeuwen, *"Kaon and open charm production in central lead-lead collisions at the CERN SPS"*, Doctoral dissertation, University of Utrecht, Netherlands, (2002).

[6] Thomas Lidlam and Larry McLerran, *"What Have We Learned From the Relativistic Heavy Ion Collider?"*, Physics Today, October 2003, pp. 48-54.

[7] Brian Aagard Peterson, *"Beauty production at HERA-B"*, Doctoral dissertation, University of Copenhagen, (2002). Available at http://www-hera-b.desy.de/tmp/2402.html.

[8] B.B. Back *et al*., *"Production of Φ Mesons in Au + Au Collisions at 11.7 A GeV/c*", arXiv:nucl-ex/0304017 v1 23 Apr 2003.

[9] David Griffiths, *"Introduction to elementary particles"*, John Willey and Sons, Inc., (1987), 392 p.

[10] P. Koch, U. Heinz and J. Pishut, *"Φ enhancement and J/Ψ suppression in nuclear collisions by rescattering of secondary hadrons"*, Physics Letters B, v. 243, 1-2, (1990), pp. 149-157.

[11] Y. Akiba *et al*. (E-802 Collaboration), *"Production of Φ Mesons in Central ^{28}Si + ^{196}Au Collisions at 14.6A GeV/c"*, Physical Review Letters, v. 76, n. 12, (1996), pp. 2021-2024.

[12] The NA49 Collaboration, *"Production of Φ meson in p+p, p+Pb and central*

Pb+Pb collisions at E_{beam} = 158 A GeV", Phys. Lett. B, v. 491, (2000), pp. 59-66.

[13] A. Alves, S. Amato, J. C. Anjos, J. A. Appel, J. Astorga, T. Bernard, S. B. Bracker, L. M. Cremaldi, W. D. Dagenhart, C. L. Darling, R. L. Dixon, D. Errede, H. C. Fenker, C. Gay, D. R. Green, R. Jedicke, P. E. Karchin, C. Kennedy, S. Kwan, L. H. Lueking, J. R. T. de Mello Neto, J. Metheny, R. H. Milburn, J. M. de Miranda, H. da Motta Filho, A. Napier, D. Passmore, A. Rafatian, A. C. dos Reis, W. R. Ross, A. F. S. Santoro, M. Shea, M. H. G. Souza, C. Stoughton, M. E. Streetman, D. J. Summers, S. F. Takach, A. Wallace, Z. Wu (Fermilab E769 Collaboration), *"Atomic mass dependence of Ξ^- and $\overline{\Xi^+}$ production in central 250 GeV π^- - nucleon interactions"*, arXiv:hep-ex/9703015 v1 28 Mar 1997.

[14] The HERA-B Collaboration, *"HERA-B: An experiment to Study CP Violation in the B system Using an Internal Target at the HERA Proton Ring. Proposal"*, DESY-PRC 94/02, (1994). Available at http://www-hera-b.desy.de/general/publications/proposal/

[15] A. Sambamurti *et al*. (Fermilab E557/E672 Collaboration), *"A-dependence of highly inelastic p-nucleus collisions"*, Physical Review D, v. 41, n. 5, (1990), pp. 1371-1383.

[16] B. K. Bondarev, A. G. Litvinenko, A. I. Malakhov, S. G. Resnikov, *"A-dependence of cumulative pions and protons production in hadron-nucleus and nucleus-nucleus collisions"*, Preprint of Joint Institute for Nuclear Research (Dubna, Russia) P1-2000-94 (2000), in Russian.

[17] O. Igonkina, *"Study of J/Ψ and χ_c meson production in proton-nucleus collisions at energy 920 GeV"*, Doctoral dissertation, ITEP, Moscow and DESY, Hamburg, (2002), in Russian.

[18] HERA-B Collaboration, *"Inclusive V^0 production cross sections from 920 GeV fixed target proton-nucleus collisions"*, Eur. Phys. J. C, v. 29, (2003), pp. 181-190.

[19] HERA-B Collaboration, *" J/Ψ production via χ_c decays in 920 GeV p-A interaction"*, Phys. Lett, v. B561, (2003), pp. 61-72.

[20] HERA-B Collaboration, *"Measurement of the $b\bar{b}$ Production Cross Section in 920 GeV Fixed-Target Proton-Nucleus Collisions"*, Eur. Phys. J. C, v. 26, (2002),

pp. 345-355.

[21] W.W.M. Allison and P.R.S. Wright, *"The Physics of Charged Particle Identification: dE/dx , Cherenkov Radiation, and Transition Radiation"*, p. 371 in *"Experimental Techniques in High Energy Physics"*, T. Ferbel, editor (Adison-Wesley, 1987).

[22] K. Hagiwata *et al.* (Particle Data Group), Phys. Rev. D, v. 66, 010001, (2002) and 2003 partial update for edition 2004.

[23] I. Arinyo, J. Bastos, D. Broemmelsiek, J. Carvalho, M. Chmeissani, P. Conde, J. Davilla, D. Dujmic, R. Eckmann, L. Garrido, D. Gascon, T. Hamacher, A. Gorisek, I. Ivaniouchenkov, M. Ispirian, S. Karabekian, M. Kim, S. Korpar, P. Krizan, S. Kupper, K. Lau, P. Maas, J. McGill, R. Miquel, N. Murthy, D. Peralta, R. Pestotnik, J. Pyrlik, S. Ramachandran, K. Reeves, J. Rosen, W. Schmidt-Parzefall, A. Schwarz, R.F. Schwitters, X. Siero, M. Staric, A. Stanovnik, D. Skrk and T. Zivko, *"The HERA-B ring imaging Cherenkov counter"*, NIM A, v. 516, n. 2-3, (2004), pp. 445-461.

[24] R. F. Schwitters, *"Single-ring Likelihood Fit Including Background"*, HERA-B note 00-021, DESY, Hamburg, 2000; available at http://www-hera-b.desy.de/notes/00/00-021.pdf.

[25] I. Arinyo, J. Bastos, D. Broemmelsiek, J. Carvalho, P. Conde, D. Dujmic, R. Eckmann, L. Garrido, A. Gorisek, I. Ivaniouchenkov, M. Ispiryan, S. Karabekyan, S. Korpar, P. Krizan, K. Lau, R. Miquel, D. Peralta, R. Pestotnik, J. Pyrlik, S. Ramachandran, K. Reeves, J. Rosen, R.F. Schwitters, M. Staric, A. Stanovnik, D. Skrk, T. Zivko, *"The HERA-B RICH"*, NIM-A, vol. 453 (2000), pp. 289-295.

[26] D. Dujmic, *"Implementation of the Unified Algorithm for RICH"*, HERA-B note 01-103, DESY, Hamburg, 2001; available at http://www-hera-b.desy.de/notes/01/01-103.pdf.

[27] P. Krizan and T. Dement, *"Search for electron rings on the photon detector of the HERA-B RICH"*, IJS Report IJS - DP - 7257, July 1998. Available at http://www-hera-b.desy.de/subgroup/detector/rich/rich/id_algorithms/hough_dp.ps.gz.

[28] M. Ispiryan and S. Ramachandran, *"Triangle Based Ring Reconstruction Algorithm for HERA-B RICH"*, HERA-B note 99-184, DESY, Hamburg 1999; available at

http://www-hera-b.desy.de/notes/99/99-184.ps.

[29] P. Krizan and M. Staric, *"An Iterative Method for the Analysis of Cherenkov Rings"*, a draft note available at http://www-hera-b.desy.de/subgroup/detector/rich/rich/id_algorithms/iterat.ps.gz.

[30] I. Arinyo and L. Garrido, *"Particle Identification with the HERA-B RICH"*, HERA-B note 99-108, DESY, Hamburg, 1999; available at http://www-hera-b.desy.de/notes/99/99-108.ps.

[31] D. Dujmic, R. Eckmann and R.F. Schwitters, *"Reconstruction of Photon Directions in the HERA-B RICH"*, HERA-B note 00-019, DESY, Hamburg, 1999; available at http://www-hera-b.desy.de/notes/00/00-019.pdf.

[32] I. Arinyo, *"Measurement of hadron fractions in Proton-Nucleus interactions at 920 GeV/c using the HERA-B detector"*, Doctoral dissertation, University of Barcelona, 2001.

[33] D. Emeliyanov, I. Kisel, S. Masciocchi, M. Sang, Yu. Vassiliev, *"Primary Vertex Reconstruction by ROVER"*, HERA-B note 00-139, DESY, Hamburg, 2000; available at http://www-hera-b.desy.de/notes/00/00-139.ps.

[34] Sylvia Masciocchi, *"Primary vertex reconstruction studies"*, HERA-B note 02-123, DESY, Hamburg, 2002.

[35] Halasya-Siva Subramania, private communication, 2003.

[36] T. J. Roberts, H. R. Gustafson, L. W. Jones, M. J. Longo and M. R. Whalley, *"Neutron-nucleus inelastic cross-section from 160 to 375 GeV/c"*, Nuclear Physics B159, (1979), pp. 56-66.

[37] P. R. V. Murthy, C. C. Ayre, H. R. Gustafson, L. W. Jones and M. J. Longo, *"Neutron total cross sections on nuclei at Fermilab energies"*, Nuclear Physics B92 (1975), pp. 269-308.

[38] A. S. Carroll, I-H. Chiang, T. F. Kycia, K. K. Li, M. D. Marx, D. C. Rahm, W. F. Baker, D. P. Earthy, G. Giacomelli, A. M. Jonckheere, P. F. M. Koehler, P. O. Mazur, R. Rubinstein, O. Fackler, *"Absorption cross sections of* π^+, K^{+-}, p *and* $\overline{p}$ *on nuclei between 60 and 280 GeV/c"*, Physics Letters, v. 80B, n. 3, (1979), pp. 319-322.

[39] J. Carvalho, *"Compilation of cross sections for proton nucleus interactions at the*

HERA energy", Nuclear Physics A, v. 725 , (2003), pp. 269-275.

[40] R. Bailey at al., *"A-dependence study of inclusive Φ production"*, NIKHEF-H/83-17, (1983).

[41] M. J. Leitch *et al*., *"Nuclear Dependence of Neutral-D-Meson Production by 800 GeV/c Protons"*, Phys. Rev. Letters, v. 72, n. 16, (1994), pp.2542-2545.

[42] M. E. J. Newman and G. T. Barkema, *"Monte Carlo Methods in Statistical Physics"*, Clarendon Press, Oxford 199, 475 p.

[43] Dave Jackson, in *"Letters"*, CERN Courier, v. 40, #1, (2003).

[44] H. Feldmeier and J. Schnack, *"Fermionic Molecular Dynamics"*, nucl-th/9703014 6 Mar 1997.

[45] Ioanis Kourbanis, *"The A-Dependence of leading particle production by 800 GeV protons"*, Doctoral dissertation, Northeastern University, Boston, Massachusetts, 1989.

[46] A. Ozawa *et al.*, *"Measurements of the interaction cross sections for Ar and Cl isotopes"*, Nuclear Physics A, v. 709 (2002), pp. 60-72.

[47] H. Geissel *et al.*, *"Experimental indication of a reduced chiral order parameter from the 1s* π^- *state in* ^{205}*Pb"*, Physics Letters B, v. 549 (2002), pp. 64-71.

[48] R. Pestotnik, *"Identification of Pions, Kaons and Protons in the HERA-B Spectrometer"*, Doctoral thesis, University of Ljubljana, 2001.

[49] R. S. Bhalerao, S. K. Gupta, P. Shukla, *"Phi-Meson Mass Modification in Heavy-Ion Collisions",* Talk given at 3rd International Conference on Physics and Astrophysics of Quark Gluon Plasma (ICPAQGP 97), Jaipur, India, 1997. e-Print Archive: hep-ph/9705332.